

Coordinated Control of Multiple UAVs: Theory and Flight Experiment.

Y. Watanabe

► To cite this version:

Y. Watanabe. Coordinated Control of Multiple UAVs: Theory and Flight Experiment.. AIAA Guidance Navigation & Control (GNC) Conference, Aug 2013, BOSTON, United States. hal-01061122

HAL Id: hal-01061122

<https://hal-onera.archives-ouvertes.fr/hal-01061122>

Submitted on 5 Sep 2014

HAL is a multi-disciplinary open access archive for the deposit and dissemination of scientific research documents, whether they are published or not. The documents may come from teaching and research institutions in France or abroad, or from public or private research centers.

L'archive ouverte pluridisciplinaire **HAL**, est destinée au dépôt et à la diffusion de documents scientifiques de niveau recherche, publiés ou non, émanant des établissements d'enseignement et de recherche français ou étrangers, des laboratoires publics ou privés.

Coordinated Control of Multiple UAVs : Theory and Flight Experiment

Yoko Watanabe*

ONERA - The French Aerospace Laboratory, Toulouse 31055, France

This paper proposes a nonlinear control law to realize a coordinated flight of multiple UAVs and evaluates its performance through flight experiments of small fixed-wing UAV platforms. Assuming all-to-all communication, a decentralized coordination control system is designed based on a virtual leader approach. The proposed control design uses a potential function defined on a phase distribution of multi agents. Two advantages of this coordination controller are; i) it can be applied to make different coordination configurations, ii) it is applicable to any number of UAVs, and so it can easily treat an event of addition/deletion of UAV units in a coordination team. The proposed coordination control law is proven to be locally asymptotically stable by using Lyapunov indirect method, and its large domain of attraction is observed in simulation. Furthermore, the controller is implemented onboard ONERA fixed-wing UAV platforms and tested with a mission scenario which includes four different coordination configurations.

I. Introduction

Coordinated operation of multiple unmanned aerial vehicles (UAVs) has aroused many researchers' interest in recent years, due to its great potential for increases in overall mission performance and robustness without augmenting a capacity of each UAV unit. The followings are some examples showing advantages of multi-UAV operation over mono-UAV one. For a surveillance mission, even though each vehicle can carry a limited number/type of sensors, data fusion of several of them distributed over an operation site in a desired configuration can provide further information and a wider sensing coverage. Communication relay can be established between vehicles to extend a range of datalink connection with a ground control station. System robustness can be improved by making redundancy so that a functional failure of one UAV among a team does not necessarily lead a mission failure. There is also an aerodynamic benefit to reduce a power consumption of each aircraft when flying in formation¹.

Various strategies for multi-agent coordination have been investigated in robotics community since many years. Especially, formation control of multiple robots, aircrafts, underwater vehicles or satellites has been intensively studied². There are two objectives in a coordination control problem. One is to make each agent maintain a desired geometric configuration with respect to others. The other is to make an entire team achieve a mission objective such as reference trajectory tracking. Two main approaches for such coordination control are i) leader-follower approach and ii) virtual structure approach. In the leader-follower approach, an agent designated as a leader takes charge of a mission objective and the other agents designated as followers maintain a desired configuration with respect to the leader. A big advantage of using this approach lies in its facility of implementation. As shown in Figure 1, the leader-follower coordination control architecture does not have any feedback loop from followers to the leader (C and D blocks in the figure denote a local controller and an agent dynamics respectively, for each agent.). This is why most of the existing work of successful UAV formation flight adopt this approach. Bayraktar et al.³ and Dong et al.⁴ realized a formation flight between two fixed-wing airplanes and between two helicopters respectively, by updating a follower's flight plan using a current leader's position in real-time on ground control station. In the work of Gu et al.⁵, three airplanes flew in formation by transmitting a leader's position directly to the two followers by radio communication. Johnson et al.⁶ developed a vision-based system onboard a follower aircraft to localize a

*Research Engineer, Systems Control and Flight Dynamics Department, Yoko.Watanabe@onera.fr

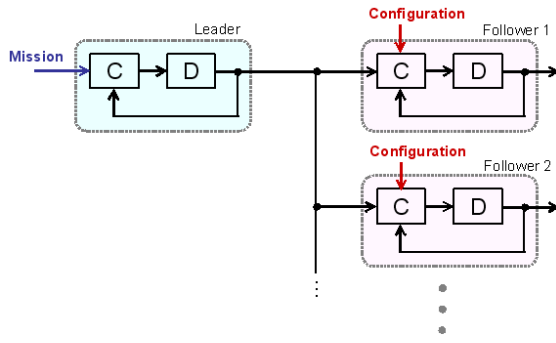


Figure 1: Leader-Follower Coordination Control Architecture

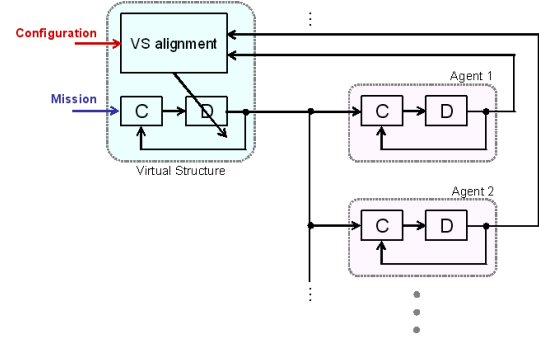


Figure 2: Virtual Structure Coordination Control Architecture

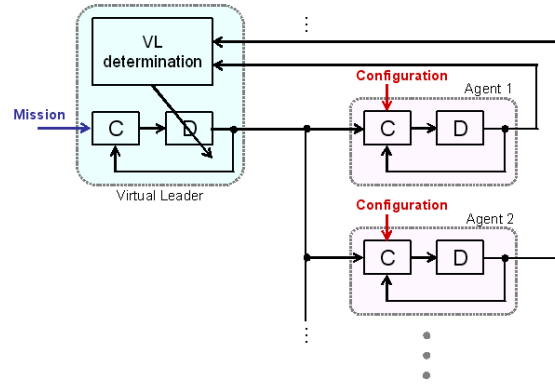


Figure 3: Virtual Leader-Follower Coordination Control Architecture

leader and achieved a two-UAV closed-loop formation flight without any communication between the UAVs. However, this leader-follower approach has a weakness in its robustness. As followers' motion is determined relative to their leader's, an error in the leader's maneuver is fully propagated to all the followers and both the mission and coordination objectives fail once losing the leader's performance.

In order to overcome this robustness issue, the virtual structure approach was introduced by Tan and Lewis⁷. Virtual structure (VS) is defined as a collection of agents, which maintains a desired geometric configuration. This approach consists of the following three steps; 1) VS is aligned with the current agent positions; 2) mission control is applied to VS to obtain a desired trajectory for each agent; and 3) each agent tracks its own desired trajectory. The mission and coordination objectives are both managed by a centralized VS control system with a feedback of every agents' states, as shown in Figure 2. However, it can be easily decentralized by duplicating the VS control system on each agent. Due to its capability to maintain a highly precise formation, many propose a spacecraft or satellite formation control law based on the VS approach⁸. For multi-UAV control application, only few work applies the VS approach. This is because of a high computational complexity of the VS position and orientation fitting from the current agents' states. Although Low and Ng⁹ suggest using a dynamic virtual structure along a maneuver-constrained trajectory for UAV formation control, it omits the first VS alignment step by assuming a given formation trajectory. So to be exact, this work does not apply the original VS approach but rather the virtual leader approach.

The virtual leader (VL) approach introduced by Leonard and Fiorelli¹⁰ is a combination of the two approaches discussed above, although it is often categorized as a family of the VS approach. Virtual leader state is determined by all the agents' current states, as a virtual structure in the VS approach. Then each agent tries to maintain a desired geometric configuration relative to the VL, as in the leader-follower approach. Figure 3 depicts a control architecture of the VL approach. Commonly, the VL position is taken at a center of mass of a team of all the agents. Hence the VL determination does not require a complex

optimization process as required in the VS alignment step. Moreover, the VL approach remains more robust than the leader-follower approach in a sense that a failure of one agent will be only partially propagated to the others via the VL position. Since the VL approaches overcome the drawbacks of both the leader-follower and the VS approaches, some have proposed its application to UAV formation flight¹¹, but not yet many examples of actual flight result using this approach can be found.

In many literatures^{2,8}, a behavioral approach is listed as the third approach of coordination control. This approach derives a control strategy as a weighted average of several different task controls such as trajectory tracking, formation keeping and obstacle avoidance¹². The coordination/formation keeping task control is essential in the behavioral approach, and it can be designed based on the two approaches mentioned above. For this reason, we prefer to distinguish this approach from the other two.

In this paper, a coordination control law for multiple UAVs is designed based on the decentralized VL approach. Inspired by a notable work of Leonard et al.¹³ and Sepulchre et al.¹⁴ on multi-agent collective motion control, we propose a controller with which each agent achieves;

- a stable circling motion at constant radius and speed around a VL position,
- a splay or synchronized phase distribution with the other agents on the circle orbit, and
- a global mission objective.

A global stability and local asymptotic stability of the desired coordination state using the proposed controller are theoretically proven by using Lyapunov direct and indirect methods. An interesting aspect of this controller is that it can be applied to make different types of coordination flight by choosing different configuration settings. For example, a splay or synchronized circling is realized by taking a fixed beacon as a virtual leader with a non-zero circling speed. Trajectory tracking in formation can be attained by taking a reference trajectory as a virtual leader with zero circling speed. We can also take a virtual leader in a conventional way, at a center of mass of the team, and use this coordination controller in combination with a VL mission controller. Another feature is that the proposed controller is applicable to any number of agents in the team. A number of agents is used as a parameter in the controller, and there is no limitation on it. This feature allows the coordination control system to handle easily an event of addition/deletion of an agent to/from the team even during operation.

The coordination controller proposed in this paper is implemented onboard three of the ONERA fixed-wing UAV platforms, shown in Figure 4, developed based on Multiplex TwinStarII R/C airplane. A mission scenario is defined by a sequence of four different coordination phases; 1) coordinated circling; 2) synchronized circling; 3) circling in formation; and 4) waypoint tracking in formation. As mentioned above, all of these phases can be realized by the same coordination control algorithm. Transitions between the phases are made autonomously by changing the configuration settings of the controller when certain conditions are satisfied. In most of the related experimental work of UAV formation flight, a transition from non-coordinated to coordinated flight phases is performed deliberately. It is often the case that a safety pilot manually places the follower UAV at a desired relative position to the leader before activating an automatic formation control^{4,5}. Unlike those work, we have achieved a completely automatic coordination flight of multiple airplane UAVs without any manual adjustment. The flight test results are shown as a highlight of this paper.

II. Multi-Agent Coordination Control

This section provides a coordination control design and its proof of stability. As stated in Section I, this paper proposes a coordination controller based on the decentralized virtual leader approach. Assuming all-to-all communication, each agent determines independently the virtual leader state and coordination control inputs by using available information on other agents' states. Before presenting the control design, an (M, N) -pattern phase distribution defined in Leonard et al.¹³ and in Sepulchre et al.¹⁴ is introduced.



Figure 4: The ONERA Fixed-Wing UAV Platforms

A. (M, N) -pattern phase distribution

Let $\boldsymbol{\theta} \in \mathbb{T}^N$ be a vector of N phase (angle) states, where $\mathbb{T} = (0, 2\pi]$. Define the m -th moment of the phase distribution $\boldsymbol{\theta}$ as follows.

$$\mathbf{p}_m(\boldsymbol{\theta}) = \frac{1}{mN} \sum_{k=1}^N \begin{bmatrix} \cos m\theta_k \\ \sin m\theta_k \end{bmatrix} \quad (1)$$

Then its potential can be defined by

$$U_m(\boldsymbol{\theta}) = \frac{N}{2} \|\mathbf{p}_m\|^2 = \frac{1}{2m^2N} \sum_{k=1}^N \sum_{j=1}^N \cos m(\theta_k - \theta_j) \quad (2)$$

Theorem II.1 *The potential U_m reaches its unique minimum of $U_m = 0$ when $\mathbf{p}_m = \mathbf{0}$, and its unique maximum of $U_m = N/2m^2$ when the phase difference between any two phases is an integer multiple of $2\pi/m$.*

Proof See *Theorem 5* in Sepulchre et al.¹⁴

Let $1 \leq M \leq N$ be a divisor of N . An (M, N) -pattern is a symmetric arrangement of N phases consisting of M clusters uniformly spaced around the unit circle, each with N/M synchronized phases. Figure 5 shows an example of the (M, N) -pattern phase distributions when $N = 12$. Then the (M, N) -potential function, denoted by $U^{M,N}$, is defined by

$$U^{M,N}(\boldsymbol{\theta}) = \sum_{m=1}^M K_m U_m(\boldsymbol{\theta}) \quad (3)$$

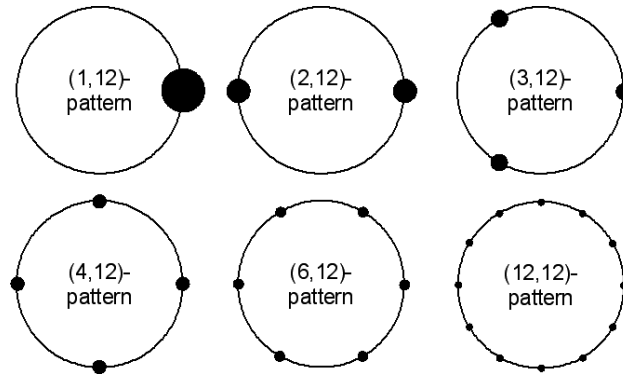


Figure 5: (M, N) -Pattern Phase Distributions (Case $N = 12$) : Size of a circle corresponds to a number of agents ($= N/M$) in a synchronized phase.

Theorem II.2 $\boldsymbol{\theta} \in \mathbb{T}^N$ is an (M, N) -pattern if and only if it is a global minimum of the potential function $U^{M,N}(\boldsymbol{\theta})$ with $K_m > 0$ for $m = 1, 2, \dots, M-1$ and $K_M < 0$.

Proof See Theorem 6 in Sepulchre et al.¹⁴

Two special cases of (M, N) -pattern phase distribution are; i) synchronized state when $M = 1$ and ii) splay state when $M = N$. In this paper, those two cases are applied to a coordination/formation control of multi-agents.

B. Coordination Control Design with Given Virtual Leader Trajectory

Let \mathbf{X}_k ($k = 1, 2, \dots, N$) and \mathbf{X}_{vl} be a 2D position of the k -th agent and a virtual leader in an inertial reference frame. Define a relative position and velocity of the k -th agent to the virtual leader by

$$\mathbf{r}_k = \mathbf{X}_k - \mathbf{X}_{vl} = r_k \begin{bmatrix} \cos \theta_k \\ \sin \theta_k \end{bmatrix} \quad (4)$$

$$\dot{\mathbf{r}}_k = \dot{\mathbf{X}}_k - \dot{\mathbf{X}}_{vl} = \dot{r}_k \begin{bmatrix} \cos \theta_k \\ \sin \theta_k \end{bmatrix} + r_k \dot{\theta}_k \begin{bmatrix} -\sin \theta_k \\ \cos \theta_k \end{bmatrix} \quad (5)$$

where $r_k \geq 0$ is distance and $\theta_k \in \mathbb{T}$ is phase. Define the following sets.

$$\begin{aligned} \mathcal{P} &= \{k \in \{1, 2, \dots, N\} \mid \mathbf{r}_k = \mathbf{0}, \dot{\mathbf{r}}_k = \mathbf{0}\} \\ \mathcal{Q} &= \{k \in \{1, 2, \dots, N\} \mid \mathbf{r}_k = \mathbf{0}, \dot{\mathbf{r}}_k \neq \mathbf{0}\} \\ \mathcal{R} &= \{k \in \{1, 2, \dots, N\} \mid \mathbf{r}_k \neq \mathbf{0}\} \end{aligned}$$

The polar coordinate system states for each set can be determined from \mathbf{r}_k and $\dot{\mathbf{r}}_k$ as shown in Table 1.

Table 1: The Polar Coordinate System States

	r_k	\dot{r}_k	θ_k	$\dot{\theta}_k$
$k \in \mathcal{P}$	0	0	unspecified	unspecified
$k \in \mathcal{Q}$	0	$\ \dot{\mathbf{r}}_k\ $	$\tan^{-1} \left(\frac{\dot{r}_{kY}}{\dot{r}_{kX}} \right)$	unspecified
$k \in \mathcal{R}$	$\ \mathbf{r}_k\ $	$\begin{bmatrix} \cos \theta_k \\ \sin \theta_k \end{bmatrix}^T \dot{\mathbf{r}}_k$	$\tan^{-1} \left(\frac{r_{kY}}{r_{kX}} \right)$	$\begin{bmatrix} -\sin \theta_k \\ \cos \theta_k \end{bmatrix}^T \frac{\dot{\mathbf{r}}_k}{r_k}$

Theorem II.3 Given a virtual leader trajectory (position, velocity and acceleration). With the following control law (6-8) for each agent, every agent's trajectory converges to a circle orbit around the virtual leader trajectory with a radius $r_o (> 0)$, an angular velocity ω_o and a phase configuration in a critical set of $U^{M,N}(\boldsymbol{\theta})$.

$$\ddot{\mathbf{X}}_k = u_{rk} \begin{bmatrix} \cos \theta_k \\ \sin \theta_k \end{bmatrix} + u_{\theta k} \begin{bmatrix} -\sin \theta_k \\ \cos \theta_k \end{bmatrix} + \ddot{\mathbf{X}}_{vl} \quad (6)$$

where

$$u_{rk} = \begin{cases} K_r r_0, & k \in \mathcal{P} \\ K_r r_0 - K_{\dot{r}} \dot{r}_k, & k \in \mathcal{Q} \\ -K_r (r_k - r_o) - K_{\dot{r}} \dot{r}_k - K_{r\theta} r_k (\dot{\theta}_k - \omega_o)^2 - r_k \dot{\theta}_k^2, & k \in \mathcal{R} \end{cases} \quad (7)$$

$$u_{\theta k} = \begin{cases} 0, & k \in \mathcal{P} \\ 2\dot{r}_k \omega_o, & k \in \mathcal{Q} \\ -\frac{1}{r_k} \left(K_{\theta} \frac{\partial U^{M,N}(\boldsymbol{\theta})}{\partial \theta_k} + K_{\dot{\theta}} (\dot{\theta}_k - \omega_o) \right) - (1 - K_{r\theta}) \dot{r}_k (\dot{\theta}_k - \omega_o) + 2\dot{r}_k \dot{\theta}_k, & k \in \mathcal{R} \end{cases} \quad (8)$$

with positive gains, and θ_k for $k \in \mathcal{P}$ is chosen so that $\partial U^{M,N}(\boldsymbol{\theta}) / \partial \theta_k = 0$. Furthermore, the splay and synchronized states are locally asymptotically stable when $M = N$ and $M = 1$, respectively.

Proof With the controller (6-8), the relative distance dynamics of the k -th agent become

$$\ddot{r}_k = \begin{cases} K_r r_0, & k \in \mathcal{P} \\ K_r r_0 - K_{\dot{r}} \dot{r}_k, & k \in \mathcal{Q} \\ -K_r (r_k - r_0) - K_{\dot{r}} \dot{r}_k - K_{r\theta} r_k (\dot{\theta}_k - \omega_0)^2, & k \in \mathcal{R} \end{cases}$$

The relative phase dynamics are not specified for $k \in \mathcal{P}$, $\dot{\theta}_k = \omega_0$ for $k \in \mathcal{Q}$, and

$$\ddot{\theta}_k = -\frac{1}{r_k^2} \left(K_{\theta} \frac{\partial U^{M,N}(\boldsymbol{\theta})}{\partial \theta_k} + K_{\dot{\theta}} (\dot{\theta}_k - \omega_0) \right) - (1 - K_{r\theta}) \frac{\dot{r}_k}{r_k} (\dot{\theta}_k - \omega_0)$$

for $k \in \mathcal{R}$. Define the system state by

$$\mathbf{x} = \begin{bmatrix} \mathbf{r} \\ \dot{\mathbf{r}} \\ \boldsymbol{\theta} \\ \dot{\boldsymbol{\theta}} \end{bmatrix}$$

where $\mathbf{r} = [r_1 \ \cdots \ r_N]^T$ and $\boldsymbol{\theta} = [\theta_1 \ \cdots \ \theta_N]^T$, and its domain by $\mathcal{D} = (\mathbb{R}^{+N} \times \mathbb{R}^N \times \mathbb{T}^N \times \mathbb{R}^N)$. The dynamic system of the state \mathbf{x} has the following limit cycle.

$$\begin{cases} r_k = r_0, \ \dot{r}_k = 0, \ \dot{\theta}_k = \omega_0 \ \forall k \in \{1, 2, \dots, N\} \\ \boldsymbol{\theta} \text{ of an } (M, N)\text{-pattern phase distribution} \end{cases} \quad (9)$$

Define a potential function as below.

$$V^{M,N}(\mathbf{x}) = \frac{1}{2K_{\theta}} \sum_{k=1}^N \left\{ K_r (r_k - r_0)^2 + \dot{r}_k^2 + r_k^2 (\dot{\theta}_k - \omega_0)^2 \right\} + U^{M,N}(\boldsymbol{\theta}) \quad (10)$$

where $U^{M,N}(\boldsymbol{\theta})$ defined in (3). This function is lower-bounded by $K_M N / 2M^2$, which is attained uniquely at the limit cycle (9). A time-derivative of this potential function $V^{M,N}(\mathbf{x})$ is derived as follows.

$$\begin{aligned} \dot{V}^{M,N}(\mathbf{x}) &= \sum_{k=1}^N \dot{\theta}_k \frac{\partial U^{M,N}(\boldsymbol{\theta})}{\partial \theta_k} + \frac{K_r}{K_{\theta}} \sum_{k=1}^N (r_k - r_0) \dot{r}_k + \frac{1}{K_{\theta}} \sum_{k=1}^N \left(\dot{r}_k (\ddot{r}_k + r_k (\dot{\theta}_k - \omega_0)^2) + r_k^2 (\dot{\theta}_k - \omega_0) \ddot{\theta}_k \right) \\ &= -\frac{K_{\dot{r}}}{K_{\theta}} \sum_{k \notin \mathcal{P}} \dot{r}_k^2 - \frac{K_{\dot{\theta}}}{K_{\theta}} \sum_{k \in \mathcal{R}} (\dot{\theta}_k - \omega_0)^2 + \omega_0 \sum_{k \notin \mathcal{P}} \frac{\partial U^{M,N}(\boldsymbol{\theta})}{\partial \theta_k} + \sum_{k \in \mathcal{P}} \dot{\theta}_k \frac{\partial U^{M,N}(\boldsymbol{\theta})}{\partial \theta_k} \end{aligned}$$

The last two terms vanish as

$$\frac{\partial U^{M,N}(\boldsymbol{\theta})}{\partial \theta_k} = 0 \text{ for } \forall k \in \mathcal{P}, \quad \sum_{k \notin \mathcal{P}} \frac{\partial U^{M,N}(\boldsymbol{\theta})}{\partial \theta_k} = \sum_{k=1}^N \frac{\partial U^{M,N}(\boldsymbol{\theta})}{\partial \theta_k} = 0$$

Hence, we have

$$\dot{V}^{M,N}(\mathbf{x}) = -\frac{K_{\dot{r}}}{K_{\theta}} \sum_{k \notin \mathcal{P}} \dot{r}_k^2 - \frac{K_{\dot{\theta}}}{K_{\theta}} \sum_{k \in \mathcal{R}} (\dot{\theta}_k - \omega_0)^2 \leq 0 \quad (11)$$

In result, the potential function $V^{M,N}(\mathbf{x})$ defined in (10) is a Lyapunov function and the limit cycle (9) is stable. Let \mathcal{S} be a set of all points in the system domain where $\dot{V}^{M,N}(\mathbf{x}) = 0$, i.e.,

$$\mathcal{S} = \left\{ \mathbf{x} \in \mathcal{D} \mid \dot{r}_k = 0 \text{ for } \forall k, \ \dot{\theta}_k = \omega_0 \text{ for } \forall k \notin \mathcal{P} \right\} \quad (12)$$

A point in an invariant set in \mathcal{S} first needs to satisfy $\ddot{r}_k = 0$ for $\forall k$, which implies $r_k = r_0$ for $\forall k$ (and hence the sets \mathcal{P} and \mathcal{Q} are null). At the same time, it also needs to satisfy $\ddot{\theta}_k = 0$ for $\forall k$, which implies the critical set of the (M, N) -potential function $U^{M,N}(\boldsymbol{\theta})$. Therefore, the largest invariant set in \mathcal{S} can be given by

$$\mathcal{M} = \left\{ \mathbf{x} \in \mathcal{S} \mid r_k = r_0, \frac{\partial U^{M,N}(\boldsymbol{\theta})}{\partial \theta_k} = 0 \text{ for } \forall k \right\}$$

From LaSalle's invariant set theorem¹⁵, every trajectory starting in \mathcal{D} approaches to the invariant set \mathcal{M} . In other words,

$$r_k \rightarrow r_0, \dot{r}_k \rightarrow 0, \dot{\theta}_k \rightarrow \omega_0 \text{ for } \forall k \in \{1, 2, \dots, N\}$$

and the phase configuration $\boldsymbol{\theta}$ converges to one in the critical set of $U^{M,N}(\boldsymbol{\theta})$ as $t \rightarrow \infty$.

Now we prove an asymptotical stability of the splay and synchronized state by using Lyapunov indirect method. Let $\delta \mathbf{x}$ be a small disturbance from the state in the limit cycle (9)) denoted by

$$\mathbf{x}^* = \begin{bmatrix} r_0 \mathbf{1} \\ \mathbf{0} \\ \boldsymbol{\theta}^* \\ \omega_0 \mathbf{1} \end{bmatrix} \quad \text{where } \mathbf{1} = \begin{bmatrix} 1 \\ \vdots \\ 1 \end{bmatrix}, \quad \mathbf{0} = \begin{bmatrix} 0 \\ \vdots \\ 0 \end{bmatrix}, \quad \boldsymbol{\theta}^* = \begin{bmatrix} \theta_1^* \\ \vdots \\ \theta_N^* \end{bmatrix}$$

Then its dynamics can be linearized as below.

$$\delta \dot{\mathbf{x}} = F(\boldsymbol{\theta}^*) \delta \mathbf{x} = \begin{bmatrix} O & I & O & O \\ -K_r I & -K_{\dot{r}} I & O & O \\ O & O & O & I \\ O & O & -\frac{K_{\theta}}{r_0^2} A(\boldsymbol{\theta}^*) & -\frac{K_{\dot{\theta}}}{r_0^2} I \end{bmatrix} \delta \mathbf{x} \quad (13)$$

where (i, j) -element of the matrix $A(\boldsymbol{\theta}^*)$ in (13) is defined by

$$A_{ij}(\boldsymbol{\theta}^*) = \left. \frac{\partial^2 U^{M,N}(\boldsymbol{\theta})}{\partial \theta_i \partial \theta_j} \right|_{\boldsymbol{\theta}=\boldsymbol{\theta}^*} = \beta_{ij}^* - \alpha_i^* \delta_{ij}, \quad \begin{matrix} i = 1, 2, \dots, N \\ j = 1, 2, \dots, N \end{matrix}$$

where δ_{ij} is the Kronecker delta and

$$\alpha_i^* = \frac{1}{N} \sum_{m=1}^M K_m \sum_{k=1}^N \cos m(\theta_k^* - \theta_i^*), \quad \beta_{ij}^* = \frac{1}{N} \sum_{m=1}^M K_m \cos m(\theta_j^* - \theta_i^*)$$

Note that, since $\beta_{ij}^* = \beta_{ji}^*$, the matrix $A(\boldsymbol{\theta}^*)$ is symmetric and so has N real eigenvalues denoted by λ_{A_j} ($j = 1, 2, \dots, N$). The matrix $F(\boldsymbol{\theta}^*)$ has eigenvalues at

$$\lambda_{r\pm} = \frac{-K_{\dot{r}} \pm \sqrt{K_{\dot{r}}^2 - 4K_r}}{2} \quad (14)$$

with multiplicity N associated with the relative distance dynamics, and also at

$$\lambda_{\theta_j\pm} = \frac{-K_{\theta} \pm \sqrt{K_{\theta}^2 - 4r_0^2 K_{\theta} \lambda_{A_j}}}{2r_0^2}, \quad j = 1, 2, \dots, N \quad (15)$$

with multiplicity 1 associated with the phase dynamics. The eigenvalues $\lambda_{r\pm}$ have a strictly negative real part for any $K_r > 0$ and $K_{\dot{r}} > 0$. Recall that λ_{A_j} is real. A real part of λ_{θ_j-} is strictly negative for any $K_{\theta} > 0$ and $K_{\dot{\theta}} > 0$. A real part of λ_{θ_j+} is strictly positive for $\lambda_{A_j} < 0$, zero for $\lambda_{A_j} = 0$ and strictly negative for $\lambda_{A_j} > 0$. Consider the cases of $\boldsymbol{\theta}^*$ being the splay and the synchronized state.

- i) **Splay state** ($M = N$) : Without loss of generality, the splay phase distribution can be represented as $\theta_k^* = 2\pi k/N$ for $k = 1, 2, \dots, N$. With this $\boldsymbol{\theta}^*$, the matrix $A(\boldsymbol{\theta}^*)$ becomes a cyclic matrix given by

$$A(\boldsymbol{\theta}^*) = \begin{bmatrix} c_0 & c_1 & \cdots & c_{N-2} & c_{N-1} \\ c_{N-1} & c_0 & c_1 & & \\ \vdots & c_{N-1} & c_0 & \ddots & \vdots \\ c_2 & & \ddots & \ddots & c_1 \\ c_1 & c_2 & \cdots & c_{N-1} & c_0 \end{bmatrix}$$

where

$$c_0 = \frac{1}{N} \sum_{m=1}^N K_m - K_N, \quad c_i = \frac{1}{N} \sum_{m=1}^N K_m \cos m i \frac{2\pi}{N}, \quad i = 1, 2, \dots, N-1$$

This cyclic matrix has the following eigenvalues and eigenvectors¹⁶.

$$\lambda_{Aj} = \sum_{k=0}^{N-1} c_k e^{ijk \frac{2\pi}{N}} \quad (16)$$

$$\mathbf{v}_{Aj} = [1 \quad e^{ij \frac{2\pi}{N}} \quad e^{i2j \frac{2\pi}{N}} \quad \dots \quad e^{i(N-1)j \frac{2\pi}{N}}]^T \quad (17)$$

for $j = 1, 2, \dots, N$. By substituting c_k into (16), λ_{Aj} is expanded as follows.

$$\begin{aligned} \lambda_{Aj} &= c_0 + \frac{1}{N} \sum_{k=1}^{N-1} \sum_{m=1}^N K_m \cos mk \frac{2\pi}{N} \cos jk \frac{2\pi}{N} \\ &= c_0 + \frac{1}{2N} \sum_{k=1}^{N-1} \sum_{m=1}^N K_m \cos(m+j)k \frac{2\pi}{N} + \frac{1}{2N} \sum_{k=1}^{N-1} \sum_{m=1}^N K_m \cos(m-j)k \frac{2\pi}{N} \\ &= c_0 + \frac{1}{2N} \sum_{l=1}^N (\bar{K}_l + \tilde{K}_l) \left(\sum_{k=1}^N \cos lk \frac{2\pi}{N} - 1 \right) \end{aligned}$$

where

$$\bar{K}_l = \begin{cases} N+l-j, & 1 \leq l \leq j \\ l-j, & j+1 \leq l \leq N \end{cases}, \quad \tilde{K}_l = \begin{cases} -l+j, & 1 \leq l \leq j-1 \\ N-l+j, & j \leq l \leq N \end{cases}$$

As we have

$$\sum_{k=1}^N \cos lk \frac{2\pi}{N} = \begin{cases} 0, & 1 \leq l \leq N-1 \\ N, & l = N \end{cases}$$

the eigenvalues λ_{Aj} becomes

$$\lambda_{Aj} = \begin{cases} \frac{1}{2}(K_j + K_{N-j} - 2K_N) > 0, & j = 1, \dots, N-1 \\ 0, & j = N \end{cases} \quad (18)$$

- ii) **Synchronized state ($M = 1$)** : For the synchronized phase distribution, $\theta_i^* = \theta_j^*$ for $\forall i \neq j$. Hence, the matrix $A(\boldsymbol{\theta}^*)$ becomes

$$A(\boldsymbol{\theta}^*) = K_1 \left(\frac{1}{N} \mathbf{1}\mathbf{1}^T - I \right)$$

By solving the characteristic equation, an eigenvalue at 0 with an eigenvector $\mathbf{v}_A = \mathbf{1}$, and $(N-1)$ eigenvalues at $-K_1 > 0$ with eigenvectors \mathbf{v}_A satisfying $\mathbf{1}^T \mathbf{v}_A = 0$ are obtained.

From the discussion above, in the both cases of the splay and synchronized states, the matrix $A(\boldsymbol{\theta}^*)$ has one zero eigenvalue and the other $(N-1)$ eigenvalues strictly positive. Also in the both cases, the eigenvector associated with the zero eigenvalue is $\mathbf{v}_A = \mathbf{1}$. This corresponds to a steady rotation within the same limit cycle (9). All the other positive eigenvalues of $A(\boldsymbol{\theta}^*)$ lead the eigenvalues $\lambda_{\theta_j \pm}$ in (15) to have a negative real part. From the Lyapunov indirect method, the limit cycle (9) of the splay and synchronized states is locally asymptotically stable when using the proposed controller (6-8) with $M = N$ and $M = 1$ respectively.

C. Coordination Control Design with Virtual Leader at Center of Mass

In Section II.B, a coordination controller is designed with a virtual leader trajectory determined independently from the agents' motion. However, in formation control problem, it is common to take a virtual leader at a center of mass of the team of agents. In this case, the VL position and velocity are given by

$$\mathbf{X}_{vl} = \frac{1}{N} \sum_{j=1}^N \mathbf{X}_j, \quad \dot{\mathbf{X}}_{vl} = \frac{1}{N} \sum_{j=1}^N \dot{\mathbf{X}}_j \quad (19)$$

This section modifies the coordination controller in Theorem II.3 by replacing a VL acceleration $\ddot{\mathbf{X}}_{vl}$ by its desired one, and analysis stability of the limit cycle (9) with the modified controller.

Theorem II.4 Define virtual leader position and velocity by (19), and suppose a controller $\ddot{\mathbf{X}}_{vl} = \mathbf{u}_d$ gives a desired VL motion. With the control law (20) for each agent, a circle orbit around the VL with a radius r_o , an angular velocity ω_o and a phase configuration in a critical set of $U^{M,N}(\boldsymbol{\theta})$ is stable. Furthermore, the splay state is locally asymptotically stable when $M = N$.

$$\ddot{\mathbf{X}}_k = u_{rk} \begin{bmatrix} \cos \theta_k \\ \sin \theta_k \end{bmatrix} + u_{\theta k} \begin{bmatrix} -\sin \theta_k \\ \cos \theta_k \end{bmatrix} + \mathbf{u}_d \quad (20)$$

where u_{rk} and $u_{\theta k}$ given in (7-8).

Proof Consider a domain $\mathcal{D}' = \{\mathbf{x} \in \mathcal{D} \mid r_k > 0 \ \forall k\}$. In this domain, with the controller (20), the relative distance and phase dynamics of the k -th agent become

$$\begin{aligned} \ddot{r}_k &= -K_r(r_k - r_o) - K_{\dot{r}}\dot{r}_k - K_{r\theta}r_k(\dot{\theta}_k - \omega_o)^2 + \begin{bmatrix} \cos \theta_k \\ \sin \theta_k \end{bmatrix}^T (\mathbf{u}_d - \ddot{\mathbf{X}}_{vl}) \\ \ddot{\theta}_k &= -\frac{1}{r_k^2} \left(K_{\theta} \frac{\partial U^{M,N}(\boldsymbol{\theta})}{\partial \theta_k} + K_{\dot{\theta}}(\dot{\theta}_k - \omega_o) \right) - (1 - K_{r\theta}) \frac{\dot{r}_k}{r_k} (\dot{\theta}_k - \omega_o) + \frac{1}{r_k} \begin{bmatrix} -\sin \theta_k \\ \cos \theta_k \end{bmatrix}^T (\mathbf{u}_d - \ddot{\mathbf{X}}_{vl}) \end{aligned}$$

Since $\mathbf{u}_d - \ddot{\mathbf{X}}_{vl} = \mathbf{0}$ when $u_{rk} = u_{\theta k} = 0$ for $\forall k$, this system also has a limit cycle described in (9) which is included in the domain \mathcal{D}' . On this limit cycle, the VL motion follows the dynamics of $\ddot{\mathbf{X}}_{vl} = \mathbf{u}_d$. Define a potential function as in (10), which has its unique minimum at the limit cycle (9). By using the relative distance and phase dynamics above, its time derivative is derived as follows.

$$\dot{V}^{M,N}(\mathbf{x}) = -\frac{K_{\dot{r}}}{K_{\theta}} \sum_{k=1}^N \dot{r}_k^2 - \frac{K_{\dot{\theta}}}{K_{\theta}} \sum_{k=1}^N (\dot{\theta}_k - \omega_o)^2 + \frac{1}{K_{\theta}} \left(\sum_{k=1}^N \dot{r}_k - \omega_o \sum_{k=1}^N r_k \begin{bmatrix} -\sin \theta_k \\ \cos \theta_k \end{bmatrix} \right)^T (\mathbf{u}_d - \ddot{\mathbf{X}}_{vl}) \quad (21)$$

From the definitions (4-5) and (19), the last term in (21) vanishes. Hence,

$$\dot{V}^{M,N}(\mathbf{x}) = -\frac{K_{\dot{r}}}{K_{\theta}} \sum_{k=1}^N \dot{r}_k^2 - \frac{K_{\dot{\theta}}}{K_{\theta}} \sum_{k=1}^N r_k^2 (\dot{\theta}_k - \omega_o)^2 \leq 0 \quad (22)$$

and the limit cycle (9) is stable.

Similarly to the previous section, an asymptotical stability of the splay state (when $M = N$) is proven by using Lyapunov indirect method. Let $\delta \mathbf{x}$ be a small disturbance from the state in the limit cycle (9) with the splay phase distribution. Then its dynamics can be linearized as below.

$$\delta \dot{\mathbf{x}} = \tilde{F}(\boldsymbol{\theta}^*) \delta \mathbf{x} = \begin{bmatrix} O & I & O & O \\ -K_r I + C_r & -K_{\dot{r}} I + C_{\dot{r}} & C_{\theta} & C_{\dot{\theta}} \\ O & O & O & I \\ D_r & D_{\dot{r}} & -\frac{K_{\theta}}{r_0^2} A(\boldsymbol{\theta}^*) + D_{\theta} & -\frac{K_{\dot{\theta}}}{r_0^2} I + D_{\dot{\theta}} \end{bmatrix} \delta \mathbf{x} \quad (23)$$

Define $N \times N$ matrices \mathcal{C} and \mathcal{S} whose (i, j) -elements are

$$\mathcal{C}_{ij} = \frac{1}{N} \cos \left((j-i) \frac{2\pi}{N} \right), \quad \mathcal{S}_{ij} = \frac{1}{N} \sin \left((j-i) \frac{2\pi}{N} \right), \quad \begin{matrix} i = 1, 2, \dots, N \\ j = 1, 2, \dots, N \end{matrix}$$

Then, the matrices C_* and D_* ($*$ = $r, \dot{r}, \theta, \dot{\theta}$) in $\tilde{F}(\boldsymbol{\theta}^*)$ are given by

$$\begin{aligned} C_r &= (K_r + \omega_o^2) \mathcal{C}, & D_r &= \frac{1}{r_0} (K_r + \omega_o^2) \mathcal{S} \\ C_{\dot{r}} &= K_{\dot{r}} \mathcal{C} + 2\omega_o \mathcal{S}, & D_{\dot{r}} &= \frac{1}{r_0} (K_{\dot{r}} \mathcal{S} - 2\omega_o \mathcal{C}) \\ C_{\theta} &= -r_0 \left(\frac{K_{\theta}}{r_0^2} \lambda_{A1} + \omega_o^2 \right) \mathcal{S}, & D_{\theta} &= \left(\frac{K_{\theta}}{r_0^2} \lambda_{A1} + \omega_o^2 \right) \mathcal{C} \\ C_{\dot{\theta}} &= 2r_0 \omega_o \mathcal{C} - \frac{K_{\dot{\theta}}}{r_0} \mathcal{S}, & D_{\dot{\theta}} &= \frac{1}{r_0} \left(2r_0 \omega_o \mathcal{S} + \frac{K_{\dot{\theta}}}{r_0} \mathcal{C} \right) \end{aligned}$$

where $\lambda_{A1} = \frac{1}{2}(K_1 + K_{N-1} - 2K_N) > 0$ given in (18). Let λ be an eigenvalue of the matrix $\tilde{F}(\theta^*)$ and \mathbf{v} be its corresponding eigenvector. Then, λ and \mathbf{v} can be obtained by solving the following equations.

$$(\lambda^2 + K_{\dot{r}}\lambda + K_r)\mathbf{v}_r = (\lambda C_{\dot{r}} + C_r)\mathbf{v}_r + (\lambda C_{\dot{\theta}} + C_{\theta})\mathbf{v}_{\theta} \quad (24)$$

$$(\lambda^2 + \frac{K_{\dot{\theta}}}{r_0^2}\lambda)\mathbf{v}_{\theta} + \frac{K_{\theta}}{r_0^2}A(\theta^*)\mathbf{v}_{\theta} = (\lambda D_{\dot{r}} + D_r)\mathbf{v}_r + (\lambda D_{\dot{\theta}} + D_{\theta})\mathbf{v}_{\theta} \quad (25)$$

where $\mathbf{v} = [\mathbf{v}_r^T \quad \lambda \mathbf{v}_r^T \quad \mathbf{v}_{\theta}^T \quad \lambda \mathbf{v}_{\theta}^T]^T$. When $N = M = 2$, we have

$$\mathcal{C} = \frac{1}{2} \begin{bmatrix} 1 & -1 \\ -1 & 1 \end{bmatrix}, \quad \mathcal{S} = O, \quad A(\theta^*) = \lambda_{A1}\mathcal{C}$$

By solving the equations (24, 25) with those matrices, the eigenvalues of the matrix $\tilde{F}(\theta^*)$ are obtained as $\lambda = 0$, $-K_{\dot{\theta}}/r_0^2$, $\lambda_{r\pm}$ with multiplicity 1, and $\lambda = \pm i\omega_0$ with multiplicity 2. When $N = M > 2$, the matrices \mathcal{C} and \mathcal{S} have the following characteristics;

$$\mathcal{C}\mathcal{S} = \mathcal{S}\mathcal{C} = \frac{1}{2}\mathcal{S}, \quad \mathcal{C}^2 = -\mathcal{S}^2 = \frac{1}{2}\mathcal{C} \quad (26)$$

which leads the relationship $D_* = 2\mathcal{S}\mathcal{C}_*/r_0$. By using this relationship in the equations (24, 25), the eigenvalues are derived by $\lambda = 0$, $-K_{\dot{\theta}}/r_0^2$, $\lambda_{\theta_j\pm}$ for $j = 2, 3, \dots, N-2$ with multiplicity 1, $\lambda = \lambda_{r\pm}$ with multiplicity $N-2$, and $\lambda = \pm i\omega_0$, $\lambda_{r\theta\pm}$ with multiplicity 2, where

$$\lambda_{r\theta\pm} = \frac{-(K_{\dot{r}} + \frac{K_{\dot{\theta}}}{r_0^2}) \pm \sqrt{(K_{\dot{r}} + \frac{K_{\dot{\theta}}}{r_0^2})^2 - 8(K_r + \frac{K_{\theta}}{r_0^2}\lambda_{A1})}}{4} \quad (27)$$

In any case, all the eigenvalues of the matrix $\tilde{F}(\theta^*)$ have a strictly negative real part except $\lambda = 0$ and $\lambda = \pm i\omega_0$. While the zero eigenvalue corresponds to a steady rotation within the same limit cycle, the eigenvalues $\lambda = \pm i\omega_0$ correspond to a translational shift of the limit cycle which was not appeared in the previous case because the VL motion was given independently from the state \mathbf{x} . From Lyapunov indirect method, the limit cycle (9) of the splay state is proven to be locally asymptotically stable with the proposed controller (20) with $M = N$.

D. Phase Constraint

In the previous two subsections, we have seen that the controllers (6, 20) stabilize a team of multi-agents on a circle orbit around a VL position with a radius r_0 and an angular velocity ω_0 , and that the splay and synchronized phase distributions are asymptotically stable. Whereas a relative phase configuration among all the agents is controlled to be a desired one with those controllers, an absolute phase trajectory cannot be specified. For example, in a case of $\omega_0 = 0$ and $M = N$, the agents will be equally distributed on a circle orbit around a virtual leader, but an orientation of the configuration is arbitrary. In this subsection, we impose a phase constraint on one of the agents in the team so that its phase trajectory tracks a given reference.

First, consider the case in which the virtual leader motion is known.

Corollary II.5 *Let θ_d be a phase reference where $\dot{\theta}_d = \omega_0$. The following controller (28) stabilizes the limit cycle (9), with a phase trajectory of the j -th agent converging to θ_d .*

$$\ddot{\mathbf{X}}_k = u_{rk} \begin{bmatrix} \cos \theta_k \\ \sin \theta_k \end{bmatrix} + \left(u_{\theta k} - \frac{\delta_{jk}}{r_j} K_{\theta_d} \sin(\theta_j - \theta_d) \right) \begin{bmatrix} -\sin \theta_k \\ \cos \theta_k \end{bmatrix} + \ddot{\mathbf{X}}_{vl} \quad (28)$$

where u_{rk} and $u_{\theta k}$ are given by (7, 8). Furthermore, the splay state is locally asymptotically stable when $M = N$.

Proof Define a new potential function by

$$W^{M,N}(\mathbf{x}) = V^{M,N}(\mathbf{x}) + \frac{K_{\theta_d}}{K_{\theta}} (1 - \cos(\theta_j - \theta_d)) \quad (29)$$

where $V^{M,N}(\mathbf{x})$ is given by (10). $W^{M,N}(\mathbf{x})$ is lower-bounded by $K_M N/2M^2$, which is attained uniquely at the limit cycle (9) with $\theta_j = \theta_d$. A time derivative of $W^{M,N}(\mathbf{x})$ can be derived as follows.

$$\dot{W}^{M,N}(\mathbf{x}) = -\frac{K_{\dot{r}}}{K_{\theta}} \sum_{k=1}^N \dot{r}_k^2 - \frac{K_{\dot{\theta}}}{K_{\theta}} \sum_{k=1}^N r_k^2 (\dot{\theta}_k - \omega_o)^2 \leq 0$$

Therefore, $W^{M,N}(\mathbf{x})$ is a Lyapunov function and the limit cycle with $\theta_j = \theta_d$ is stable.

An asymptotical stability of the splay state can be also proven. Consider a small disturbance $\delta\mathbf{x}$ from the desired splay state with the phase constraint $\theta_j = \theta_d$. Its dynamics can be linearized as below.

$$\delta\dot{\mathbf{x}} = G(\boldsymbol{\theta}^*)\delta\mathbf{x} = \begin{bmatrix} O & I & O & O \\ -K_r I & -K_{\dot{r}} I & O & O \\ O & O & O & I \\ O & O & -\frac{K_{\theta}}{r_0^2} A(\boldsymbol{\theta}^*) - \frac{K_{\theta_d}}{r_0^2} \mathbf{e}_j \mathbf{e}_j^T & -\frac{K_{\dot{\theta}}}{r_0^2} I \end{bmatrix} \delta\mathbf{x} \quad (30)$$

The eigenvalues of $G(\boldsymbol{\theta}^*)$ associated with the relative distance dynamics remains the same as those of $F(\boldsymbol{\theta}^*)$ given in (14). Those associated with the relative phase dynamics need to satisfy

$$(\lambda^2 + \frac{K_{\dot{\theta}}}{r_0^2} \lambda) \mathbf{v}_{\theta} + \frac{K_{\theta}}{r_0^2} A(\boldsymbol{\theta}^*) \mathbf{v}_{\theta} + \frac{K_{\theta_d}}{r_0^2} \mathbf{e}_j \mathbf{e}_j^T \mathbf{v}_{\theta} = \mathbf{0} \quad (31)$$

Without loss of generality, we can take $j = 1$ and $\theta_d = 2\pi/N$. Suppose $\mathbf{v}_{\theta} = \sum_{k=1}^N \alpha_k \mathbf{v}_{A_k} \neq \mathbf{0}$, where \mathbf{v}_{A_k} given in (17). By using the fact of $\sum_{k=1}^N \mathbf{v}_{A_k}/N = \mathbf{e}_1$, the equation above becomes

$$\sum_{k=1}^N \left((\lambda^2 + \frac{K_{\dot{\theta}}}{r_0^2} \lambda + \frac{K_{\theta}}{r_0^2} \lambda_{A_k}) \alpha_k + \frac{K_{\theta_d}}{r_0^2} \bar{\alpha} \right) \mathbf{v}_{A_k} = \mathbf{0} \quad (32)$$

where $\bar{\alpha} = \sum_{k=1}^N \alpha_k/N$ and λ_{A_k} given by (18). This is satisfied when α_k for $k = 1, 2, \dots, N$ is chosen so that every coefficients in (32) are zero. When $\bar{\alpha} = 0$, the following condition is required for any $k = 1, 2, \dots, N$.

$$\alpha_k = 0 \quad \text{or} \quad \lambda^2 + \frac{K_{\dot{\theta}}}{r_0^2} \lambda + \frac{K_{\theta}}{r_0^2} \lambda_{A_k} = 0$$

This happens only when $\alpha_{N-i} = -\alpha_i \neq 0$ ($i < N/2$) and all the other α_k 's are zero. Such α 's give eigenvalues of $\lambda = \lambda_{\theta_i \pm}$ with multiplicity 1. Now suppose $\bar{\alpha} \neq 0$. By taking $\alpha_N = 1$ without loss of generality, we have

$$\lambda^2 + \frac{K_{\dot{\theta}}}{r_0^2} \lambda + \frac{K_{\theta_d}}{r_0^2} \bar{\alpha} = 0 \quad (33)$$

$$\alpha_k = \frac{K_{\theta_d} \bar{\alpha}}{K_{\theta_d} \bar{\alpha} - K_{\theta} \lambda_{A_k}} = \frac{\bar{\alpha}}{\bar{\alpha} - K'_{\theta} \lambda_{A_k}}, \quad k = 1, 2, \dots, N-1 \quad (34)$$

where $K'_{\theta} = K_{\theta}/K_{\theta_d} > 0$. By substituting this α_k in the definition of $\bar{\alpha}$ and by multiplying it by $\prod_{i=1}^{N-1} (\bar{\alpha} - K'_{\theta} \lambda_{A_i})$, $\bar{\alpha}$ can be obtained by solving the following N th-order polynomial equation.

$$(N\bar{\alpha} - 1) \left(\prod_{i=1}^{N-1} (\bar{\alpha} - K'_{\theta} \lambda_{A_i}) \right) - \bar{\alpha} \sum_{k=1}^{N-1} \left(\prod_{i=1, i \neq k}^{N-1} (\bar{\alpha} - K'_{\theta} \lambda_{A_i}) \right) = N \left(\bar{\alpha}^N + \sum_{i=0}^{N-1} (-1)^{N-i} f_i \bar{\alpha}^i \right) = 0 \quad (35)$$

where the coefficients $f_i > 0$ for all $i = 0, 1, \dots, N-1$ since $K'_{\theta} > 0$ and $\lambda_{A_k} > 0$ for $k = 1, 2, \dots, N-1$. The equation (35) has $(N+1)/2$ solutions for odd N and $(N/2+1)$ solutions for even N since $\alpha_k = \alpha_{N-k}$, and they are all strictly positive. The eigenvalues of $G(\boldsymbol{\theta}^*)$ associated with each solution $\bar{\alpha}$ can be obtained from (33), and they have a strictly negative real part since $\bar{\alpha} > 0$. Therefore, the splay state with $\theta_j = \theta_d$ is locally asymptotically stable. It should be noted that the zero eigenvalue disappeared because the phase constraint will be violated after the steady rotation.

Now we consider the case in which the VL position is given by a center of mass of the team of multi-agents.

Corollary II.6 *VL position and velocity are defined by (19). The following controller (36) stabilizes the limit cycle (9) with $\theta_j = \theta_d$ and the VL motion following $\dot{\mathbf{X}}_d = \mathbf{u}_d$.*

$$\ddot{\mathbf{X}}_k = u_{rk} \begin{bmatrix} \cos \theta_k \\ \sin \theta_k \end{bmatrix} + \left(u_{\theta k} - \frac{\delta_{jk}}{r_j} K_{\theta_d} \sin(\theta_j - \theta_d) \right) \begin{bmatrix} -\sin \theta_k \\ \cos \theta_k \end{bmatrix} + \mathbf{u}_d \quad (36)$$

where u_{rk} and $u_{\theta k}$ are given by (7, 8). Furthermore, the splay state is locally asymptotically stable when $M = N$.

Proof Consider a domain $\mathcal{D}' = \{\mathbf{x} \in \mathcal{D} \mid r_k > 0 \ \forall k\}$ which includes the limit cycle. Define a potential function as in (29). Similarly to the proofs of Theorem II.4 and Corollary II.5, $W^{M,N}(\mathbf{x})$ is a Lyapunov function and the limit cycle with $\theta_j = \theta_d$ is stable.

Consider the case $M = N$. Dynamics of the small disturbance from the desired splay state with the phase constraint $\theta_j = \theta_d$ can be linearized as follows.

$$\delta \dot{\mathbf{x}} = \bar{G}(\boldsymbol{\theta}^*) \delta \mathbf{x} = \begin{bmatrix} O & I & O & O \\ -K_r I + C_r & -K_{\dot{r}} I + C_{\dot{r}} & \bar{C}_{\theta} & C_{\dot{\theta}} \\ O & O & O & I \\ D_r & D_{\dot{r}} & -\frac{K_{\theta_d}}{r_0^2} A(\boldsymbol{\theta}^*) - \frac{K_{\theta_d}}{r_0^2} \mathbf{e}_j \mathbf{e}_j^T + \bar{D}_{\theta} & -\frac{K_{\dot{\theta}}}{r_0^2} I + D_{\dot{\theta}} \end{bmatrix} \delta \mathbf{x} \quad (37)$$

where C_* and D_* ($*$ = $r, \dot{r}, \theta, \dot{\theta}$) are defined in Section II.C, and

$$\bar{C}_{\theta} = C_{\theta} - \frac{K_{\theta_d}}{r_0} \mathcal{S} \mathbf{e}_j \mathbf{e}_j^T, \quad \bar{D}_{\theta} = D_{\theta} + \frac{K_{\theta_d}}{r_0^2} \mathcal{C} \mathbf{e}_j \mathbf{e}_j^T$$

Without loss of generality, we take $j = 1$ and $\theta_d = 2\pi/N$.

When $N = M = 2$, the matrix $\bar{G}(\boldsymbol{\theta}^*)$ has eigenvalues of $\lambda = \lambda_{r\pm}$,

$$\lambda_{\theta_d \pm} = \frac{-K_{\dot{\theta}} \pm \sqrt{K_{\dot{\theta}}^2 - 2r_0^2 K_{\theta_d}}}{2r_0^2}$$

with multiplicity 1 and $\lambda = \pm i\omega_0$ with multiplicity 2. When $N = M > 2$, recall that we have relationships of (26) and $D_* = 2\mathcal{S}C_*/r_0$ which holds for the new matrices \bar{C}_{θ} and \bar{D}_{θ} . The eigenvalues associated purely with the relative distance dynamics (i.e., $\mathbf{v}_{\theta} = \mathbf{0}$) remain the same as those of the matrix $\bar{F}(\boldsymbol{\theta}^*)$, which is $\lambda = \lambda_{r\pm}$ with multiplicity $N - 2$. The eigenvalues associated purely with the relative phase dynamics need to satisfy the equation (31) as well as $(\lambda C_{\dot{\theta}} + \bar{C}_{\theta})\mathbf{v}_{\theta} = \mathbf{0}$. The two equations give the eigenvalues of $\lambda_{\theta_i \pm}$ defined in (15) when $\mathbf{v}_{\theta} = \mathbf{v}_{A_i} - \mathbf{v}_{A_{N-i}}$ for $2 \leq i < N/2$. Now consider the eigenvalues associated with the coupled distance-phase dynamics. From the properties of \mathcal{C} and \mathcal{S} given in (26), we obtain the equation $\mathcal{C}\mathbf{v}_r = \mathbf{v}_r/2$ which leads to $\mathbf{v}_r = \alpha_1 \mathbf{v}_{A_1} + \alpha_{N-1} \mathbf{v}_{A_{N-1}} \neq \mathbf{0}$. Suppose $\mathbf{v}_{\theta} = \sum_{k=1}^N \beta_k \mathbf{v}_{A_k}$, then λ , α_1 , α_{N-1} and β_k 's can be derived by solving

$$((\lambda^2 - \omega_0^2) - i2\lambda\omega_0)(\alpha_1 - ir_0\beta_1)\mathbf{v}_{A_1} + ((\lambda^2 - \omega_0^2) + i2\lambda\omega_0)(\alpha_{N-1} + ir_0\beta_{N-1})\mathbf{v}_{A_{N-1}} = \mathbf{0} \quad (38)$$

$$\sum_{k=1}^N \left((\lambda^2 + \frac{K_{\dot{\theta}}}{r_0^2} \lambda + \frac{K_{\theta}}{r_0^2} \lambda_{A_k}) \beta_k + \frac{K_{\theta_d}}{r_0^2} \bar{\beta} \right) \mathbf{v}_{A_k} = \frac{i}{r_0} (\lambda^2 + K_{\dot{r}} \lambda + K_r) (\alpha_1 \mathbf{v}_{A_1} - \alpha_{N-1} \mathbf{v}_{A_{N-1}}) \quad (39)$$

where $\bar{\beta} = \sum_{k=1}^N \beta_k/N$. (38) is satisfied either i) when $\lambda = i\omega_0$ and $\beta_{N-1} = i\alpha_{N-1}/r_0$, ii) when $\lambda = -i\omega_0$ and $\beta_1 = -i\alpha_1/r_0$, or iii) when $\beta_1 = -i\alpha_1/r_0$ and $\beta_{N-1} = i\alpha_{N-1}/r_0$. (39) is satisfied if $\gamma_k = 0$ for $\forall k$, where

$$\gamma_k = (\lambda^2 + \frac{K_{\dot{\theta}}}{r_0^2} \lambda + \frac{K_{\theta}}{r_0^2} \lambda_{A_k}) \beta_k + \frac{K_{\theta_d}}{r_0^2} \bar{\beta} + \begin{cases} -\frac{i}{r_0} (\lambda^2 + K_{\dot{r}} \lambda + K_r) \alpha_1, & k = 1 \\ +\frac{i}{r_0} (\lambda^2 + K_{\dot{r}} \lambda + K_r) \alpha_{N-1}, & k = N - 1 \\ 0, & \text{otherwise} \end{cases}$$

When $\bar{\beta} = 0$, the two equations are satisfied only in the case of iii) with $\beta_1 = -\beta_{N-1}$ and $\beta_k = 0$ for $k = 2, 3, \dots, N - 2, N$. In this case, the eigenvalues are given by $\lambda = \lambda_{r\theta \pm}$ in (27). Now suppose $\bar{\beta} \neq 0$. In the case of i),

$$\frac{K_{\theta_d}}{r_0^2} \bar{\beta} = \frac{i}{r_0} \left(2\omega_0^2 - K_r - \frac{K_{\theta}}{r_0^2} \lambda_{A_1} - i\omega_0 (K_{\dot{r}} + \frac{K_{\dot{\theta}}}{r_0^2}) \right) \alpha_{N-1}$$

By substituting this into the equation $\gamma_k = 0$ for $k = 1, 2, \dots, N-2, N$ and using the definition of $\bar{\beta}$, all the coefficients β_k 's and α_1 are solved in function of α_{N-1} . In the similar way, an eigenvector for $\lambda = -i\omega_0$ can be derived in the case of ii). In the case of iii), we have $\alpha_1 = -\alpha_{N-1}$ and

$$\frac{K_{\theta_d}}{r_0^2} \bar{\beta} = \frac{i}{r_0} \left((\lambda^2 + K_{\dot{r}} \lambda + K_r) + (\lambda^2 + \frac{K_{\dot{\theta}}}{r_0^2} \lambda + \frac{K_{\theta}}{r_0^2} \lambda_{A_1}) \right) \alpha_1$$

By substituting this into the equation $\gamma_k = 0$, β_k can be written by

$$\beta_k = -\frac{i}{r_0} \frac{(\lambda^2 + K_{\dot{r}} \lambda + K_r) + (\lambda^2 + \frac{K_{\dot{\theta}}}{r_0^2} \lambda + \frac{K_{\theta}}{r_0^2} \lambda_{A_1})}{\lambda^2 + \frac{K_{\dot{\theta}}}{r_0^2} \lambda + \frac{K_{\theta}}{r_0^2} \lambda_{A_k}} \alpha_1, \quad k = 2, 3, \dots, N-2, N$$

From the definition of $\bar{\beta}$, λ is obtained by solving

$$\left((\lambda^2 + K_{\dot{r}} \lambda + K_r) + (\lambda^2 + \frac{K_{\dot{\theta}}}{r_0^2} \lambda + \frac{K_{\theta}}{r_0^2} \lambda_{A_1}) \right) \left(N \frac{r_0^2}{K_{\theta_d}} + \sum_{k=2}^{N-2, N} \frac{1}{\lambda^2 + \frac{K_{\dot{\theta}}}{r_0^2} \lambda + \frac{K_{\theta}}{r_0^2} \lambda_{A_k}} \right) + 2 = 0 \quad (40)$$

Since $\lambda_{A_k} = \lambda_{A_{N-k}} > 0$ and all the gains are strictly positive, this equation becomes a stable (or Hurwitz) polynomial of order $2(N/2+2)$ for even N and of order $2((N-1)/2+2)$ for odd N . That is, all the solutions λ have a strictly negative real part. In summary, when $N = M > 2$, the matrix $\bar{G}(\theta^*)$ has eigenvalues of $\lambda_{\theta_i \pm}$ for $i = 2, \dots, N/2-1$ or $(N-1)/2$, $\lambda_{r\theta \pm}$, $\pm i\omega_0$ and the $(N+4)$ or $(N+3)$ solutions of the equation (40) with multiplicity 1, and of $\lambda_{r\pm}$ with multiplicity $(N-2)$.

Again in any case, all the eigenvalues of $\bar{G}(\theta^*)$ have a negative real part except $\lambda = \pm i\omega_0$. From Lyapunov indirect method, the splay state with $\theta_j = \theta_d$ is locally asymptotically stable.

III. Numerical Simulation

This section demonstrates numerical simulation results which validate the theorems and the corollaries introduced in Section II. Four examples with different coordination configurations are presented.

A. Example 1 : Splay circling around a fixed beacon

In the first example, a virtual leader is given by a fixed beacon at a known position $\mathbf{X}_{vl} = \mathbf{0}$ (m). By using the control law (6), five agents are controlled to keep a splay state ($M = N$) around this fixed beacon with circling radius $r_0 = 50$ (m) and angular velocity $\omega_0 = 0.3$ (rad/sec). The initial position and velocity for each agent are given by normally distributed random values, with standard deviations of 50 (m) and 1 (m/sec) respectively. Control gains used in this simulation are;

$$K_r = 1, \quad K_{\dot{r}} = 3\sqrt{K_r}, \quad K_{\theta} = \frac{r_0^2}{2} K_r, \quad K_{\dot{\theta}} = 1.4r_0^2 \sqrt{K_r}, \quad K_{r\theta} = 1,$$

and $K_m = 1$ for $m = 1, 2, \dots, N-1$ and $K_N = -1$. With those gains, the relative distance dynamics around the limit cycle have a natural frequency of 1 and a damping ratio 1.5. The relative phase dynamics have a natural frequency 1 and a damping ratio 0.7. Figure 6(a) shows trajectory profile for each agent. It is seen that their states converge to the desired splay state at $t = 13$ (sec). Figure 6(b) is a time history of the potential functions $U^{M,N}(\theta)$ and $V^{M,N}(\mathbf{x})$ defined in (3) and (10). The difference $V^{M,N}(\mathbf{x}) - U^{M,N}(\theta)$ represents a sum of the distance and angular velocity tracking errors. The Lyapunov function $V^{M,N}(\mathbf{x})$ converges to its minimum value $-K_N/2N$, which is attained uniquely at the desired splay state.

B. Example 2 : Synchronized circling around a fixed beacon with phase constraint

The second example uses the same settings as the first example, except that the desired phase configuration is a synchronized circling ($M = 1$). In addition, the phase constraint $\theta_d(t) = \omega_0 t$ (rad) is imposed on the agent 1. Each agent motion is controlled by the controller (28) with the control gain $K_{\theta_d} = K_{\theta}$. Figure 7 shows trajectory profiles, relative distance and phase of each agent to the fixed beacon position, and the potential functions $U^{M,N}(\theta)$, $V^{M,N}(\mathbf{x})$ and $W^{M,N}(\mathbf{x})$ defined in (29). The difference $W^{M,N}(\mathbf{x}) - V^{M,N}(\mathbf{x})$

corresponds to the phase reference tracking error of the agent 1. From the phase plot, one can see that a phase trajectory of the agent 1 (in blue) converges to its reference (in yellow). At the same time, the phases of the other agents get to be synchronized and also converge to the reference. This convergence can be observed clearly also in the plot of $W^{M,N}(\mathbf{x})$ which goes to its minimum.

C. Example 3 - Splay state around a moving beacon with phase constraint

The third example also uses the controller (28) with the phase constraint $\theta_d = 0$ (rad) on the agent 1. The desired state in this example is a splay state ($M = N$) around a moving beacon with a radius $r_0 = 50$ (m) and zero angular velocity $\omega_0 = 0$ (rad/sec). Let \mathbf{X}_{ref} , $\dot{\mathbf{X}}_{ref}$ and $\ddot{\mathbf{X}}_{ref}$ be a reference position, velocity and acceleration for the beacon. Then, motion of the beacon is controlled to track this reference, independently from the agents' motion, by using the following PD controller.

$$\ddot{\mathbf{X}}_{vl} = -K_p(\mathbf{X}_{vl} - \mathbf{X}_{ref}) - K_d(\dot{\mathbf{X}}_{vl} - \dot{\mathbf{X}}_{ref}) + \ddot{\mathbf{X}}_{ref}, \quad K_p = 1, \quad K_d = 3 \quad (41)$$

In the simulation, the circle reference trajectory

$$\mathbf{X}_{ref}(t) = 100 \begin{bmatrix} \cos 0.4t \\ \sin 0.4t \end{bmatrix} \quad (42)$$

is chosen. The initial position and velocity of the beacon are all zero. Figure 8(a) illustrates trajectories of the five agents and the moving beacon. Figure 8(b) shows profiles of distance and phase of each agent relative to the beacon. The agents' states are converging to the desired phase-constrained splay state.

D. Example 4 : Splay state around a center of mass with phase constraint

In the three examples presented above, the VL motion was completely known, and so are the relative distance and phase dynamics of each agent. In this fourth example, the VL position and velocity are given by a center of mass of the agents, i.e., by (19). Here we take over the same simulation settings as used in Example 3. A desired VL acceleration \mathbf{u}_d is determined in the same manner as in (41) with the circle reference trajectory (42). It should be noted that the real VL acceleration $\ddot{\mathbf{X}}_{vl}$ does not necessary coincide with \mathbf{u}_d . Each agent motion is controlled by the controller (36) with the phase constraint $\theta_1 = \theta_d = 0$ (rad). The simulation results are shown in Figure 9. Every agents' states converge to the phase-constrained splay state, and in addition, the motion of their center of mass (=virtual leader) follows its desired one. Figure 9(d) compares the VL desired and real accelerations (\mathbf{u}_d in red dashed vs. $\ddot{\mathbf{X}}_{vl}$ in blue solid), and shows that the difference between the two vanishes.

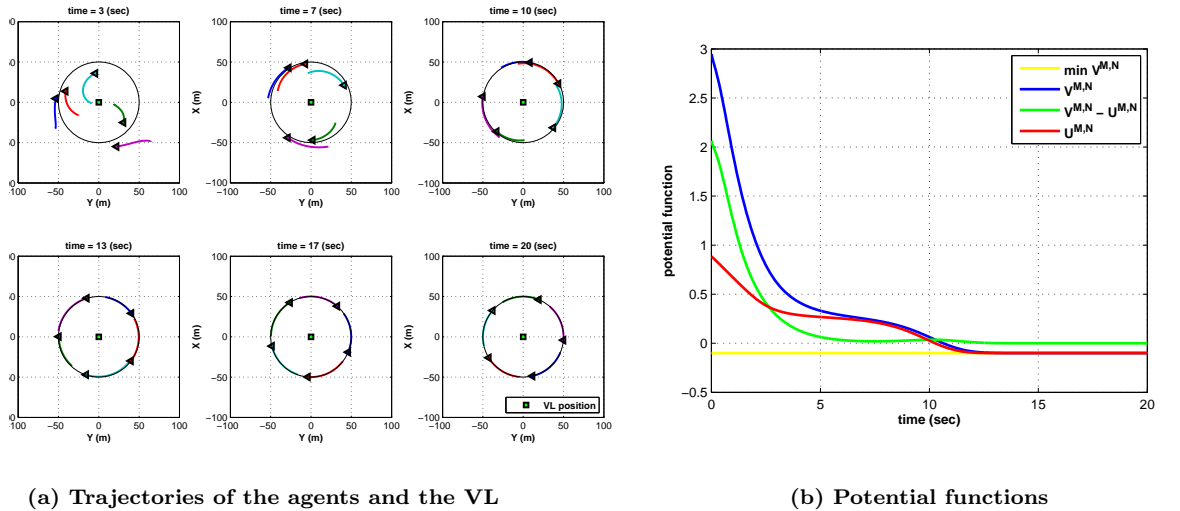
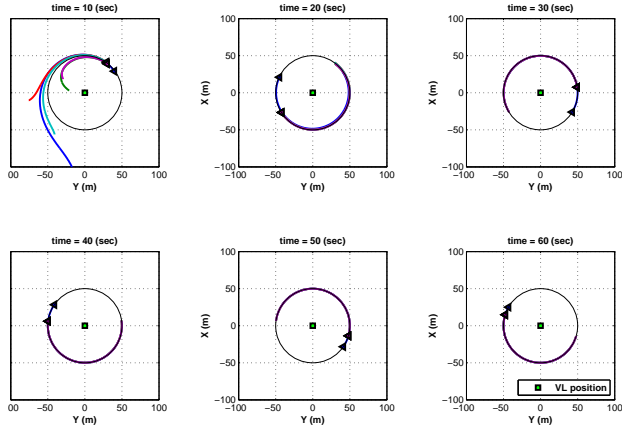
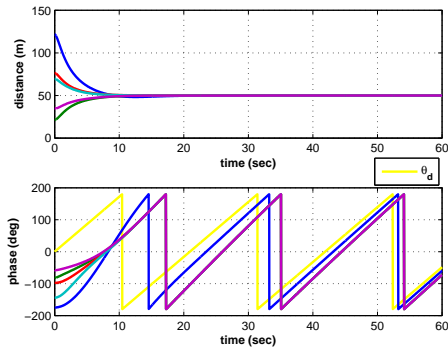


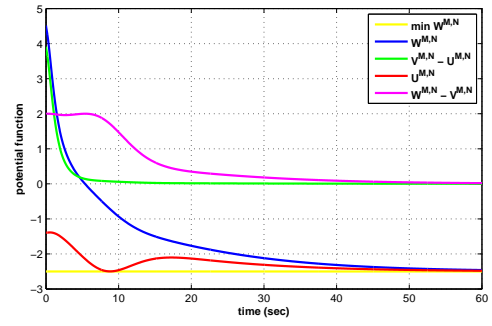
Figure 6: Example 1 - Five agents circling around a fixed beacon with splay state



(a) Trajectories of the agents and the VL

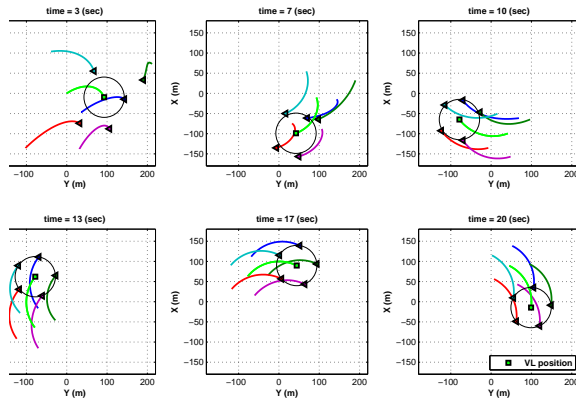


(b) Distance and phase of each agent

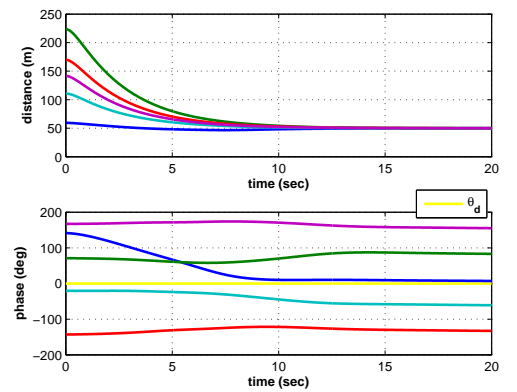


(c) Potential functions

Figure 7: Example 2 - Five agents circling around a fixed beacon with synchronized state

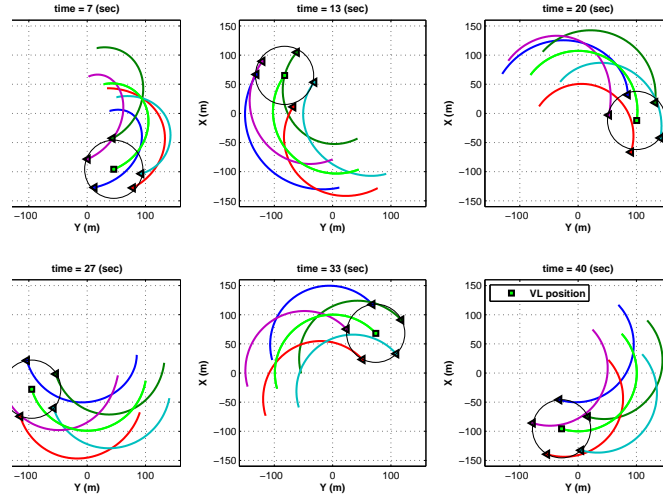


(a) Trajectories of the agents and the VL

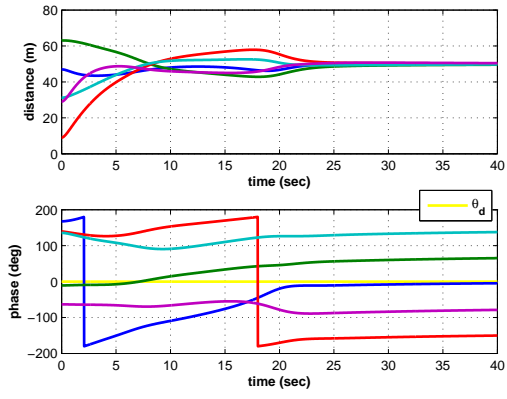


(b) Distance and phase of each agent

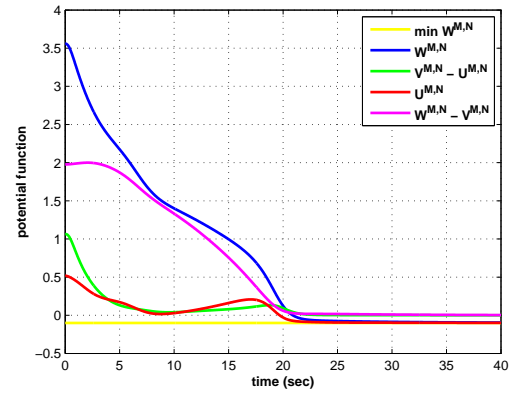
Figure 8: Example 3 - Five agents in phase-constrained splay state around a moving beacon



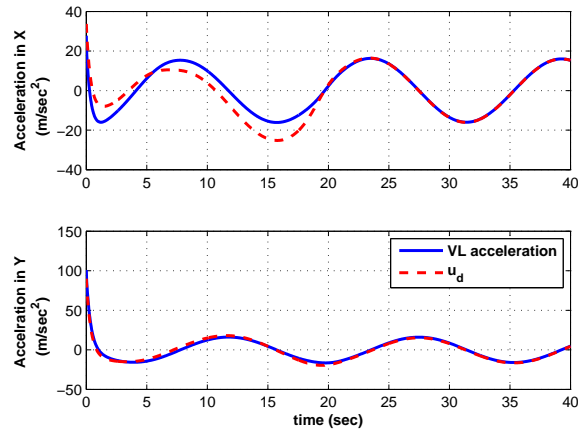
(a) Trajectories of the agents and the VL



(b) Distance and phase of each agent



(c) Potential functions



(d) Desired and real VL accelerations

Figure 9: Example 4 - Five agents in phase-constrained splay state around their center of mass

E. Conclusion of Numerical Simulation

The proposed coordination controller has been tested through simulations with different configurations;

- different numbers of agents (N)
- the splay, synchronized and other (M, N) -pattern phase distributions
- with zero and non-zero angular velocities
- with or without phase constraint
- the VL position at a fixed/moving beacon and at a center of mass of the agents

When M takes different values from 1 and N , we have seen several cases that the agent states converge to a phase distribution in the critical set of $U^{M,N}(\theta)$ other than the (M, N) -pattern. Figure 10 shows such a case. In this simulation, the controller (6) is applied to six agents with $M = 2$. The desired phase distribution for this case is $(2, 6)$ -pattern where two groups of three agents have opposite phases. However, as seen in Figure 10, the agents end up with a group of two and a group of four having opposite phases. The potential functions $V^{M,N}(x)$ and $U^{M,N}(\theta)$ are not reaching at their minimum value. Throughout simulations, such a convergence failure has not been observed for cases of $M = 1$ and $M = N$. In conclusion, even though the *almost global* asymptotical stability of the limit cycle with the splay or synchronized state is not theoretically proven, its very large domain of attraction is empirically shown. Only problem identified in simulation is that u_{θ_k} becomes very large when having a large r_0 and nearly-zero r_k . This problem can be avoided by taking a small margin $\delta r > 0$ for the classifications to the sets \mathcal{P} and \mathcal{Q} .

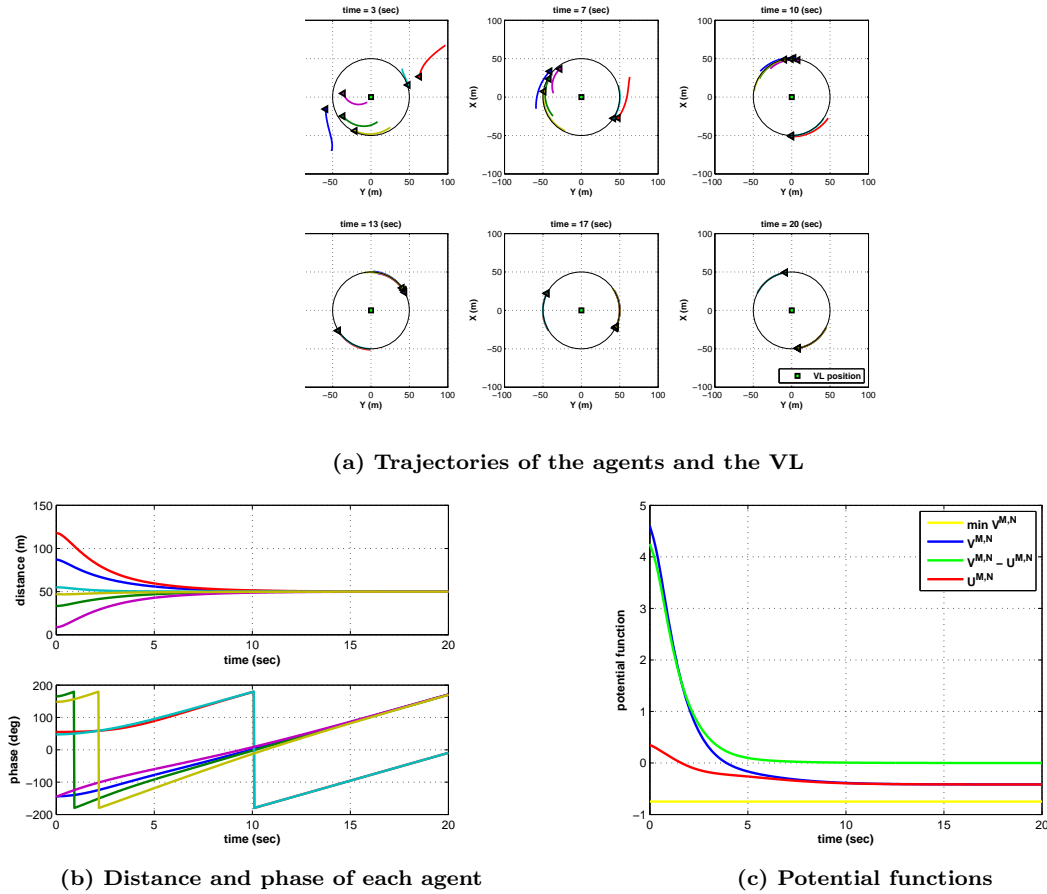


Figure 10: Counter-example of convergence : Six agents circling around a fixed beacon, not converging to $(2, 6)$ -pattern phase distribution

IV. Coordinated Flight of Multiple UAVs

In this section, the coordination controllers designed in Section II and validated in Section III is applied to a mission of coordinated flight of multiple fixed-wing UAVs. The section first defines the entire mission scenario, then describes how to realize the onboard coordination control system architecture.

A. Mission Scenario

A global objective of the mission defined in this work is to make multiple UAVs track a flight plan, given by a sequence of waypoints ($WP1 \rightarrow WP2 \rightarrow \dots$), in formation. The mission scenario consists of the following five phases.

- **Phase 0 - Take-off :** Each UAV is launched at any timing and follows the automatic take-off procedure until it reaches at a given fixed point (WP0). During this take-off phase, an UAV operates without any coordination with other UAVs.
- **Phase 1 - Coordinated circling :** Once a UAV reaches within a certain distance to the point WP0, it starts to make a circling motion around a fixed point (defined by WP0) with a constant speed and radius while making a splay state configuration with other UAVs who are already in Phase 1 (if any). It is achieved by applying the control law (6) with $M = N$ where N is a number of UAVs in Phase 1 and is re-counted at each communication update. The VL position is given by the fixed circle center position. This phase is considered as a waiting phase for all UAVs in the team to be launched in the air and to be ready for the formation flight.
- **Phase 2 - Synchronized circling :** After all UAVs in the team are in Phase 1, either an operator or a decision-making algorithm can trigger a transition from the waiting phase to the formation phase. For a purpose of bringing all the UAVs close each other before making a formation, each UAV is commanded to make a synchronized state configuration on the circle orbit. The transition from Phase 1 to Phase 2 is realized simply by changing a value of M from N to 1 in the control law (6).
- **Phase 3 - Circling in formation :** When all the UAVs in the team assemble within a certain distance on the circle, they start to make a formation by applying the control law (20), or (36) if one wish to impose a phase constraint, with $M = N$ and $\omega_0 = 0$. $r_0 > 0$ determines a formation distance between adjacent UAVs. In this phase, the VL position are defined by a mean of the UAV positions as in (19). A control law for the VL motion (i.e., $\ddot{\mathbf{X}}_{vl} = \mathbf{u}_d$) is designed independently from the coordination control law so that it makes the same circling motion as in Phase 1 and 2.
- **Phase 4 - Waypoint tracking in formation :** A departing point is defined on the circle in function of the circle position (WP0) and the first waypoint of the track (WP1). When the team of the UAVs reaches at this departing point, it quits the circle and departs for tracking a given sequence of the waypoints ($WP1 \rightarrow WP2 \rightarrow \dots$) while keeping the formation. The transition from Phase 3 to 4 is realized by switching the control law for the VL motion from circling to waypoint tracking without any change in the coordination control law.

B. Decentralized Flight Control System Architecture

The coordination control system architecture is designed based on the one already developed onboard our fixed-wing UAV platform for mono-use, which is illustrated in Figure 11(a). The system consists of the three components; i) mission/waypoint management which deals with flight mode and waypoint changes, ii) guidance law which calculates speed, heading and altitude commands to achieve a given flight mode/waypoint, and iii) control law which calculates UAV actuator inputs from the guidance commands. This nominal control system architecture is modified as shown in Figure 11(b) so that it allows coordination control with other UAVs. Note that a navigation filter which estimates the UAV current state from available onboard sensors and its feed-back loops to each component in the control system are omitted in those figures.

The coordination control law is incorporated in the system in a decentralized manner. That is, each UAV receives states of every other UAVs in the team via communication, manages the coordination phase, and calculates the VL position and the coordination control commands by its own. As our coordination controller is designed to compute the 2D acceleration command, it is converted to the horizontal velocity

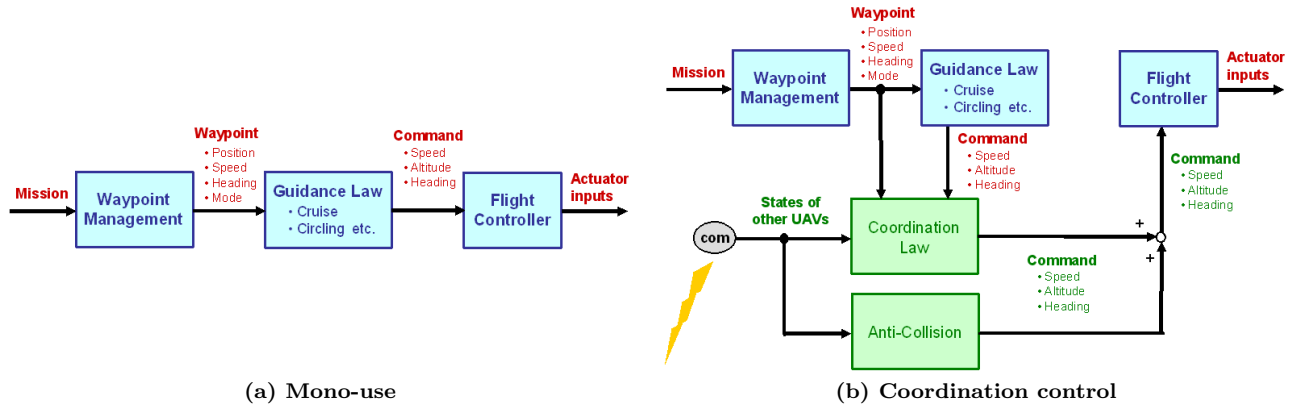


Figure 11: UAV Onboard Flight Control System Architecture

(speed+heading) command by integration. The altitude command is maintained constant at its desired value. Besides the coordination control law, an anti-collision controller is added to assure UAV flight safety. It is very important to have this component especially for Phase 2, in which the UAVs try to get together. The anti-collision controller is designed based on an artificial potential method, and is activated only when the UAV gets closer to another UAV than a certain safety minimum distance. The guidance commands for coordination and for anti-collision are combined into one, and then sent to the flight controller.

C. 6 DoF Flight Simulation

A 6 DoF flight simulator has been developed by ONERA/DCSD to mainly test performances of new guidance and control laws and flight management systems before implementing them onboard our UAV platform for their in-flight validation. This simulator is realized as a C++ program and it includes;

- a simple flight dynamics model of a fixed-wing aircraft
- measurement models of onboard sensors (GPS, INS, barometer, etc.)
- flight safety and mission management system
- navigation filter for localization
- guidance law for available flight modes
- flight controller
- 3D OpenGL graphics and interactive user interface

In this work, the simulator is first extended to simulate multiple UAVs at the same time. Then the coordination control architecture shown in Figure 11(b) is implemented in it. The mission scenario for coordination control is pre-defined in the program, and transitions between the phases listed in Section IV.A are managed by a coordination phase management function. Figure 12 is a screen shot of the interface of this simulator, on which three fixed-wing UAVs are flying in formation. The interface accepts user's input for flight mode changes, and a transition from Phase 1 to 2 is triggered by a user in the simulation.

Figure 13 is a cutoff animation of the 6 DoF flight simulation for the entire mission scenario with three UAVs. It shows the transitions of the coordination phases until the mission of waypoint tracking in formation (Phase 4) is achieved. In this simulation, a phase constraint of $\theta_j = 0$ is imposed on one of the UAVs, who locates the closest to the zero-phase position relative to the VL. Figure 14 presents the resulting altitude, speed, and control inputs (throttle, aileron, elevator and rudder) of each UAV. The speed plot shows that each UAV regulates a speed within its limit to coordinate with the other UAVs during Phase 1 and Phase 2. Figure 15 is a profile of the potential functions for each coordination phase. At each phase, the (M, N) -pattern potential function $U^{M,N}(\theta)$ (in red) tends to converge to its global minimum (in yellow), which means that the desired phase distribution is attained. In the formation flight (Phase 3 and 4), the formation tracking error (in green) and the reference phase tracking error (in magenta) are also converging to zero.

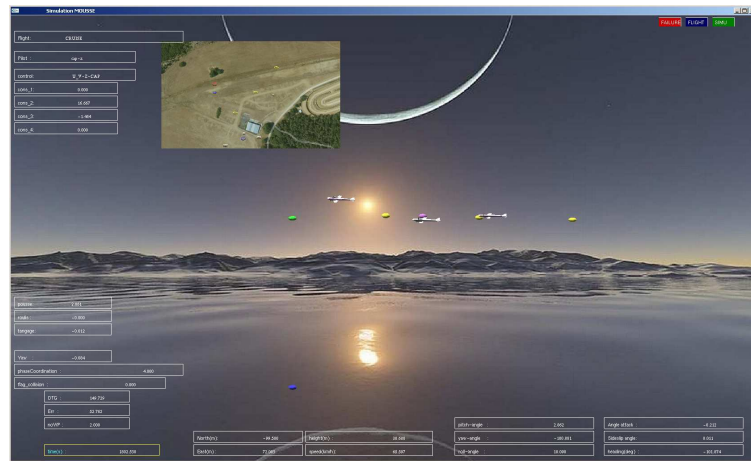


Figure 12: 6 DoF Flight Simulator for Coordination Control

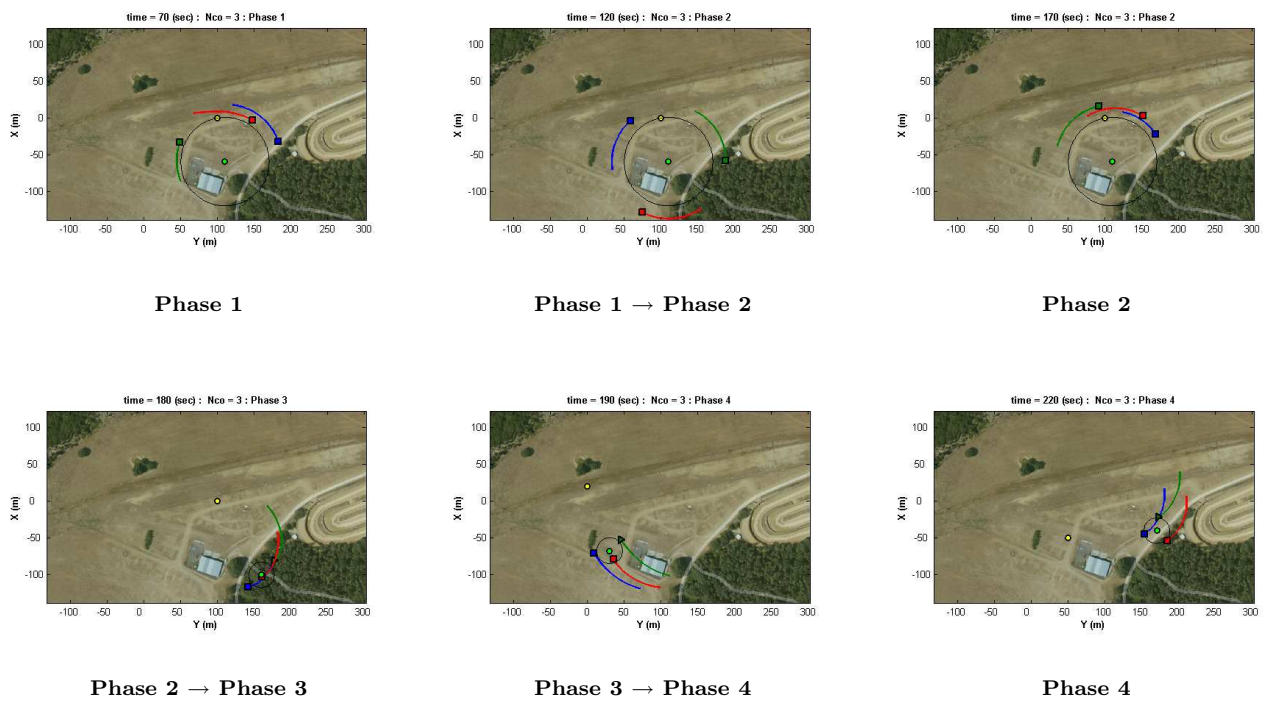


Figure 13: 6DoF Simulation Results - Trajectories of the UAVs and the VL

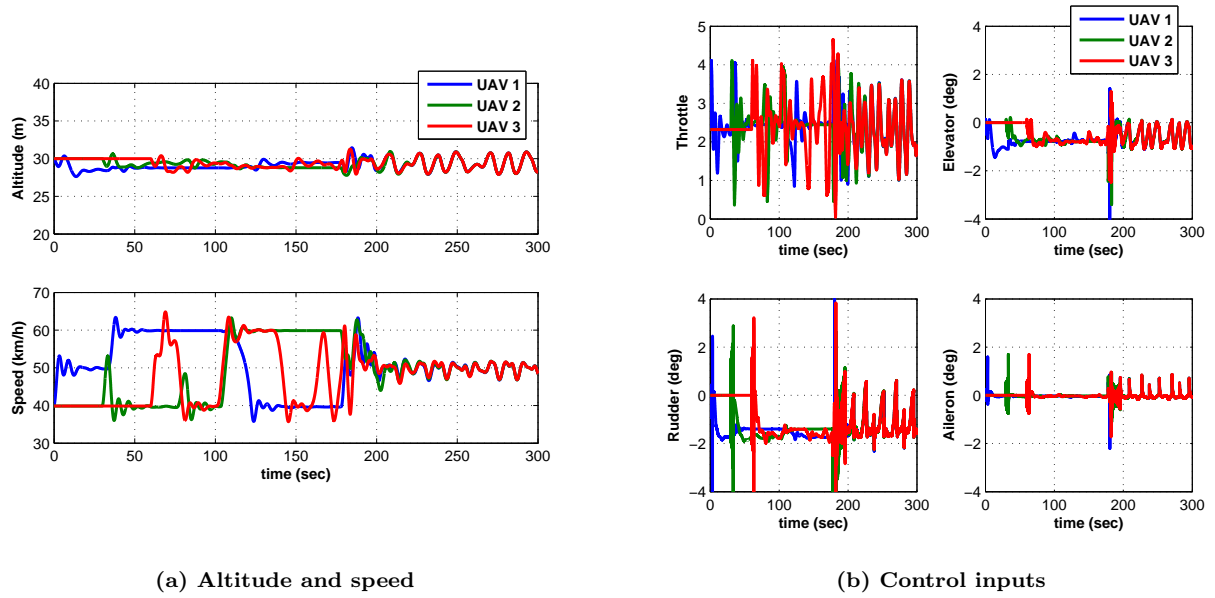


Figure 14: 6 DoF Simulation Results - Altitude, Speed and Control inputs

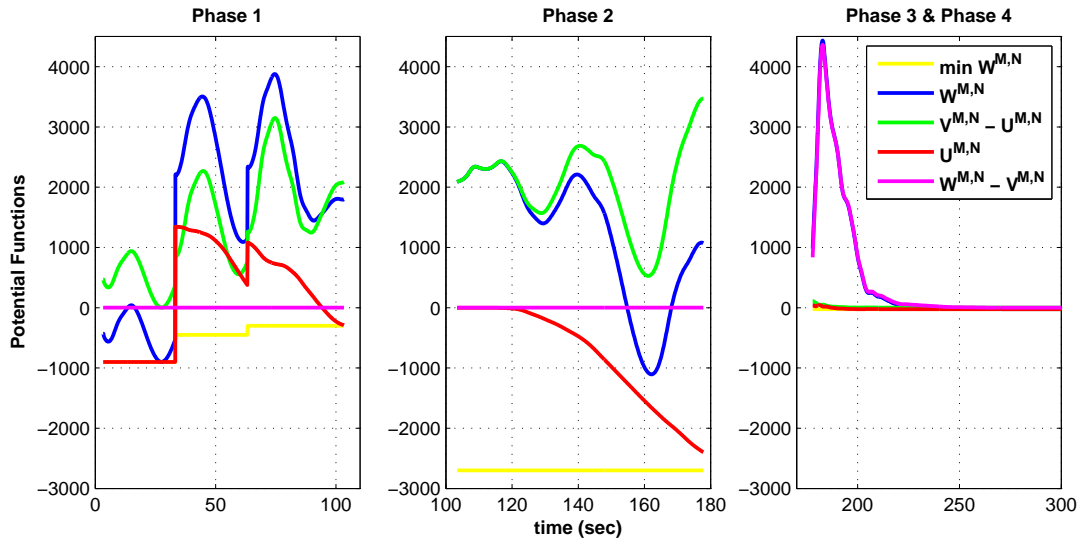


Figure 15: 6 DoF Simulation Results - Potential Functions

D. UAV Platform and Onboard System

After the validation through 6 DoF flight simulation, the proposed coordination controller has been implemented and tested onboard the ONERA ReSSAC MOUSSE fixed-wing UAV platforms (Figure 4). This platform is developed based on the R/C airplane Multiplex Twinstar II. Its specifications are summarized in Table 2.

Table 2: Specifications

Empty weight	0.8 (kg)
Take-off weight	2 (kg)
Fuselage length	1 (m)
Wingspan	1.4 (m)
Motor	electric×2
Payload	0.5 (kg)
Payload power supply	10 (W)
Flight duration	40 (min)

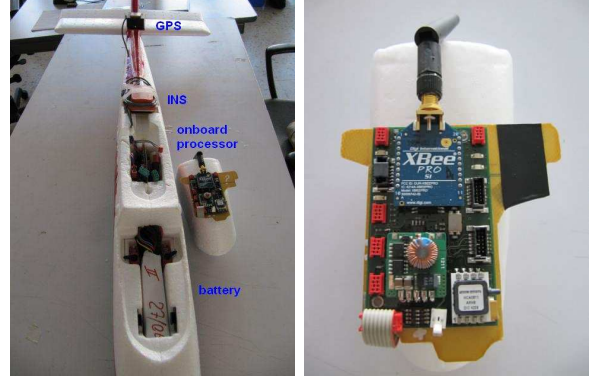


Figure 16: Onboard Hardware

Figure 16 shows the onboard hardware system of the UAV. It is equipped with Xsens MTi inertial measurement units and μ blox LEA-6H GPS. Two ARM7 micro processors (AT91SAM7) are embedded on the UAV; i) Processor CS (Switch Computer) takes charge of the radio command from a security pilot of the UAV, and ii) Processor CC (Control Computer) is dedicated to automatic flight navigation, guidance and control. The two processors are communicating each other via CAN bus datalink. The onboard hardware system includes a Xbee wireless module which is used for communications with ground control station to downlink the flight state for data recording, and also with other UAVs to exchange the state data for coordination control. Figure 17 illustrates the onboard system architecture of the ReSSAC MOUSSE UAV. The software implementation on the processors CS and CC is done in C++ program. The flight avionics system (on the processor CC) consists of functions of flight management, mission management, communication, flight navigation, guidance and control. All of these functions run in sequence with a periodic cycle of 50 (Hz). In this work, functions of the coordination phase management and of the coordination control are added in this sequence. They are programmed to perform only at 10 (Hz), once in every 5 iterations of the main-loop. The wireless communication function is also added in the sequence so that data exchange with other UAVs performs at 8.5 (Hz), once in every 6 iterations.

The ground control station (GCS) for multi UAVs has been also developed for this work. The developed GCS program is executed in Linux system on a laptop computer, and it communicates with all the UAVs in operation via wireless connection at 8.5 (Hz). On its interface, trajectories of every UAVs are displayed in a main 3D scene window, and several important states (position, velocity, attitude, flight mode, battery level etc.) of each UAV are shown separately in other windows. All the state data received from UAVs are recorded on the GCS. Although we are not currently using the uplink connection from the GCS to UAVs, there is a possibility to add it to send some commands and requests directly from the GCS without passing through radio command of the safety pilot.

E. Flight Experiment

Several flight experiments have been successfully conducted to perform the entire mission scenario defined in Section IV.A by three of our UAVs. Here presented the results obtained from the flight test on 22nd July, 2013. In this flight, three UAVs achieved a completely automatic flight in coordination from Phase 0 (automatic take-off) to Phase 4 (waypoint tracking in formation) except the transition from Phase 1 to Phase 2 triggered by an operator on ground via radio command. The flight plan is given by four waypoint positions; WP0 defines the waiting zone (Phase 1-3), and WP1, WP2 and WP3 define the formation flight circuit (Phase 4). During the waiting and transition phases (Phase 1-2), the UAVs are controlled to make a circling motion with a radius $r_0 = 60$ (m) and a constant speed $V_0 = 55$ (km/h), which gives an angular velocity $\omega_0 = 0.25$ (rad/sec). For the formation flight phases (Phase 2-4), the formation distance between the two UAVs is set at 30 (m), and a phase constraint $\theta_j = 0$ is imposed so that the UAVs aligns in North-South

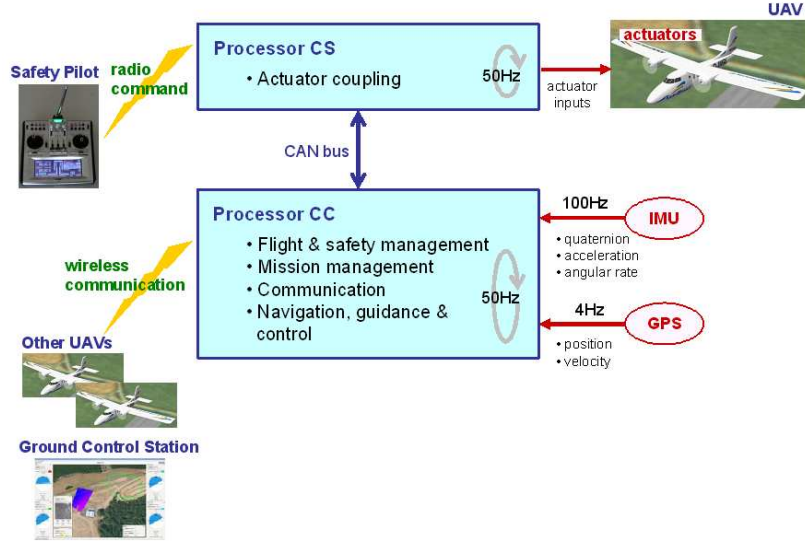


Figure 17: Onboard System Architecture

directions. In the flight, three UAVs flew at three different altitudes, 50, 70 and 90 (m) for security reason. The coordination between the three is made only for their horizontal 2D positions.

Figure 18 is a cut-off animation of the flight, which illustrates the transitions of the coordination phases. In each figure, positions of the UAVs, the VL, and the waypoints are shown. First, two UAVs made a coordinated circling, then the third one joined them on the circle (Phase 1). Triggered by an operator, the three UAVs got close each other on the circle (Phase 2) before making a formation (Phase 3). Finally, they left for the mission of waypoint tracking while maintaining a formation (Phase 4). Figure 19(a) is a time profile of the distance of each UAV to the VL shown with its desired value r_0 . Figure 19(b) compares the real and minimum value of the (M, N) -potential function $U^{M,N}(\theta)$. For each phase of the coordination, the potential function goes to its minimum. It means that the UAVs attains a desired phase distribution (splay or synchronized states). The commanded formation distance of 30 (m) is maintained with a precision of ± 10 (m). This precision can be still improved by synchronizing GPS measurements on every UAVs, by taking into account a time delay of communication, by better regulating the control gains etc.

V. Conclusion

This paper proposed the decentralized coordination controller for multiple UAVs based on the virtual leader approach. The controller design uses a potential function on phase distribution, which attains its global minimum at the desired splay/synchronized state. The first part of this paper provided a stability analysis of the proposed coordination controller and its validation through numerical simulations. Then, the second half described the application of the controller to a fully autonomous formation flight of multiple UAVs. As a highlight of this paper, the flight experiment results of three UAVs formation were presented. In some flight tests, incoherent decisions between the UAVs were observed due to communication failure. In order to overcome this consensus issue of the decentralized system, a supervision function which monitors a coordination phase management state of every UAV should be added to the system.

Acknowledgments

The author appreciates Alexandre Amiez, Paul Chavent and Pierre Escalas in the ONERA ReSSAC UAV research team for their efforts to develop our UAV platforms and the onboard hardware/software systems. Without their work, the flight experiments would not have been conducted.

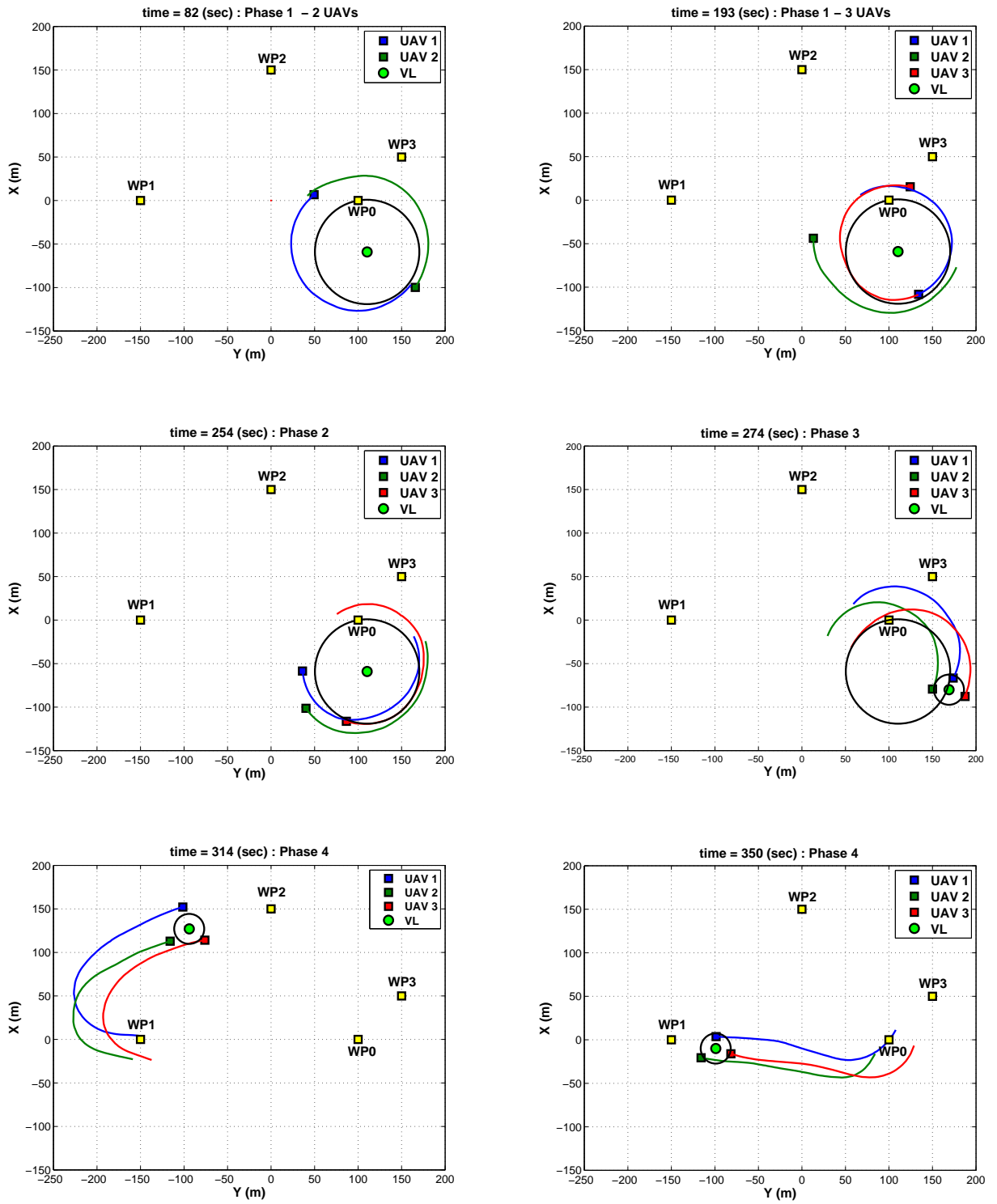
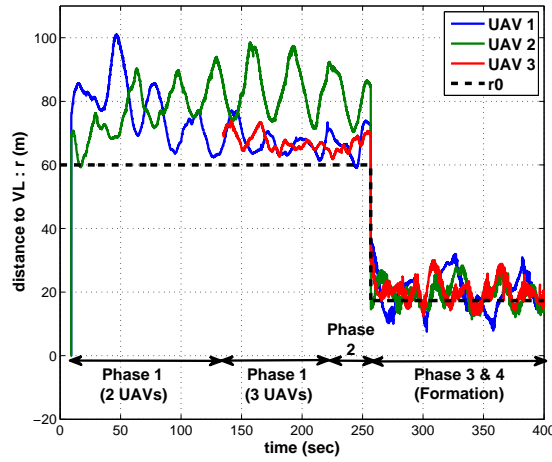
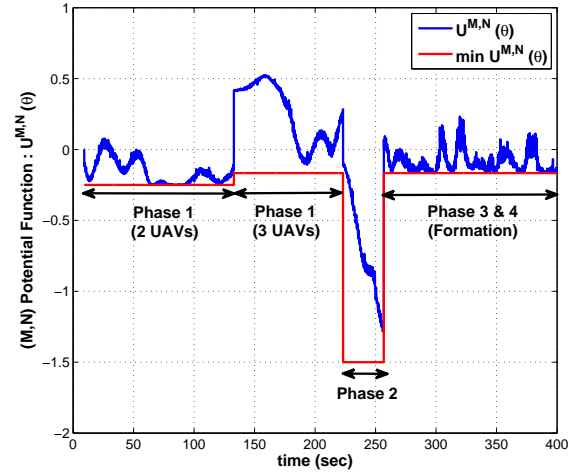


Figure 18: Flight Test Results - Trajectories of the UAVs and the VL



(a) Distance of each UAV to the VL



(b) (M, N) -Potential Function

Figure 19: Flight Test Results - Distance of each UAV to the VL and (M, N) -Potential Function

References

- ¹A. Gopalarathnam. Aerodynamic Benefit of Aircraft Formation Flight. *Encyclopedia of Aerospace Engineering*, John Wiley & Sons Ltd., 2010.
- ²Y.Q. Chen and Z. Wang. Formation Control : A review and A New Consideration. *IEEE/RSJ International Conference on Intelligent Robots and Systems*, 2005.
- ³S. Bayraktar, G.E. Fainekos and G.J. Pappas. Experimental Cooperative Control of Fixed-Wing Unmanned Aerial Vehicles. *IEEE Conference on Decision and Control*, 2004.
- ⁴X. Dong, G. Cai, F. Lin, B.M. Chen, H. Lin and T.H. Lee. Implementation of Formation Flight of Multiple Unmanned Aerial Vehicles. *IEEE International Conference on Control and Automation*, 2010.
- ⁵Y. Gu, G. Campa, B. Seanor, S. Gururajan and M.R. Napolitano. Autonomous Formation Flight - Design and Experiments. *Aerial Vehicles*, chapter 12, Intech, 2009.
- ⁶E.N. Johnson, A.J. Calise, Y. Watanabe, J. Ha and J.C. Neidhoefer. Real-Time Vision-Based Relative Aircraft Navigation. *AIAA Journal of Aerospace Computing, Information and Communication*, volume 4, 2007.
- ⁷K.H. Tan and M.A. Lewis. Virtual Structures for High-Precision Cooperative Mobile Robotic Control. *IEEE/RSJ International Conference on Intelligent Robots and Systems*, 1996.
- ⁸W. Ren and R.W. Beard. Decentralized Scheme for Spacecraft Formation Flying via the Virtual Structure Approach. *AIAA Journal of Guidance, Control and Dynamics*, volume 27, no 1, 2004.
- ⁹C.B. Low and Q.S. Ng. A Flexible Virtual Structure Formation Keeping Control for Fixed-Wing UAVs. *IEEE International Conference on Control and Automation*, 2011.
- ¹⁰N.E. Leonard and E. Fiorelli. Virtual Leaders, Artificial Potentials and Coordinated Control of Groups. *IEEE Conference on Decision and Control*, 2001.
- ¹¹T. Hino. Simple Formation Control Scheme Tolerant to Communication Failures for Small Unmanned Air Vehicles. *International Congress of the Aeronautical Sciences*, 2010.
- ¹²T. Balch and R.C. Arkin. Behavior-based Formation Control for Multi-Robot Team. *IEEE Transactions on Robotics and Automation*, volume 14, no 6, 1998.
- ¹³N.E. Leonard, D.A. Palay, F. Lekien, R. Sepulchre, D.M. Fratantoni and R.E. Davis. Collective Motion, Sensor Networks, and Ocean Sampling. *Proceedings of the IEEE*, volume 95, no 1, 2007.
- ¹⁴R. Sepulchre, D.A. Palay and N.E. Leonard. Stabilization of Planar Collective Motion: All-to-All Communication. *IEEE Transactions on Automatic Control*, volume 52, no 5, 2007.
- ¹⁵H.K. Khalil. Nonlinear Systems (Third Edition). Prentice Hall Inc., 2002.
- ¹⁶K. Okuda. Variety and Generality of Clustering in Globally Coupled Oscillators. *Physica D*, volume 63, no 3-4, 1993.